ACS Catalysis

Review

pubs.acs.org/acscatalysis

Distinguishing Homogeneous from Heterogeneous Water Oxidation Catalysis when Beginning with Polyoxometalates

Jordan J. Stracke and Richard G. Finke*

Chemistry Department, Colorado State University, Fort Collins, CO 80523, United States

ABSTRACT: Polyoxometalates (POMs) have been proposed to be excellent homogeneous water oxidation catalysts (WOCs) due to their oxidative stability and activity. However, recent literature indicates that even these relatively robust compounds can be transformed into heterogeneous, metal-oxide WOCs under the oxidizing reaction conditions needed to drive O_2 evolution. This review covers the experimental methodology for distinguishing homogeneous and heterogeneous WOCs; it then addresses the "what is the true catalyst?" problem for POMs used as precatalysts in the oxidation of water to O_2. These results are also compared to the broader WOC literature. The primary findings in this review are the following: (1) Multiple, complementary experiments are needed to determine the true catalyst, including determination of catalyst stability, speciation, and kinetics under operating conditions. (2) Controls with hypothetical heterogeneous metal-oxide catalysts are required to determine their kinetic competence in the reaction and support the conclusion of either a homogeneous or heterogeneous catalyst. (3) Although many studies observe qualitative stability of the starting POM under the reaction conditions, there is a lack of quantitative stability studies; if one does not know where the (pre)catalyst mass lies, then it is very difficult to rule out the possibility of an alternative species as the true catalyst. (4) The stability of POMs is dependent on the polyoxometalate, the metal center, and the reaction conditions. And, (5) as a result of the variable stability of POMs under different reaction conditions, those different conditions can influence the dominant catalyst identity. Overall, knowledge of which POMs (or other starting materials) tend to transform into heterogeneous WOCs, and how they do so, is therefore critical to developing the next generation of higher stability, higher activity, and truly long-lived POM and other water oxidation catalysts.

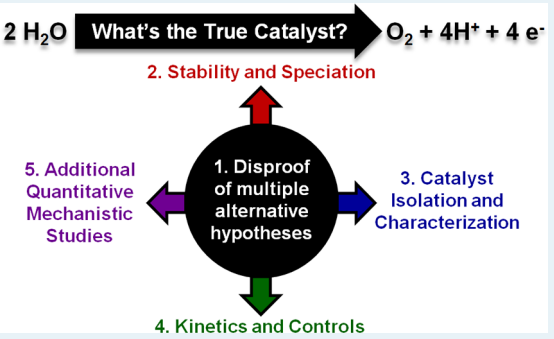

KEYWORDS: *water oxidation catalyst, polyoxometalate, homogeneous versus heterogeneous, oxygen evolution, oxidation kinetics*

1. INTRODUCTION

Catalysis is as important a discipline as any in the chemical sciences. It is directly involved in the production of numerous chemicals and materials. Recent estimates indicate catalysis is involved in producing 90% of industrial chemicals.[1]

Due to the economic and fundamental scientific impact of catalysis, knowledge of the true catalyst is of utmost importance in catalysis science. Restated, because all catalytic properties are derived directly from the identity of the active catalyst—including activity, selectivity, lifetime, poisoning, isolability, and catalyst regeneration—one must first identify the active catalyst in order to optimize and improve that catalyst. A subtopic of the catalyst identification problem is distinguishing homogeneous from heterogeneous catalysts. This topic has been reviewed both generally[2,3] and in a variety of specific areas, including cross coupling,[4] hydrogenation,[5] water splitting,[6] and water oxidation[7] reactions. Recently, the problem of identifying the true catalyst has come to a head in the water oxidation literature, where a number of systems which begin with discrete precursors are transformed into heterogeneous metal-oxide catalysts under the highly oxidizing environments needed for catalytic water oxidation. Current interest in water oxidation derives from the importance this reaction promises to play in sustainable energy storage schemes such as water splitting[8−19] and the reduction of CO_2 to fuels[20−25] such as methanol. The water oxidation half-reaction is often cited as a bottleneck in these fuel forming cycles due to the complexity of this net four electron, four proton transfer reaction along with the requirements of high activity, long lifetime, and affordability of the catalyst. Numerous reports of water oxidation and solar water splitting devices have begun addressing these challenges and have been reviewed.[26−37]

However, and despite the explosion of research in the area of water oxidation by discrete precursors, only recently has the problem of distinguishing homogeneous and heterogeneous catalysis become a priority. Recent reviews have addressed this problem in a broad manner for water oxidation catalysis.[6,7] The first of these provides a general discussion of determining water oxidation catalysts by focusing on a handful of case studies.[7] The second review[6] discusses water splitting with discussion of WOCs as well as reduction catalysts—an area which has been reviewed previously,[3] although not in the specific area of H_2 evolution. The main conclusions of the prior reviews in the area of distinguishing homogeneous and heterogeneous WOCs are the following: (i) Conditions are important in determining the

Received: December 9, 2013
Revised: January 17, 2014
Published: February 14, 2014

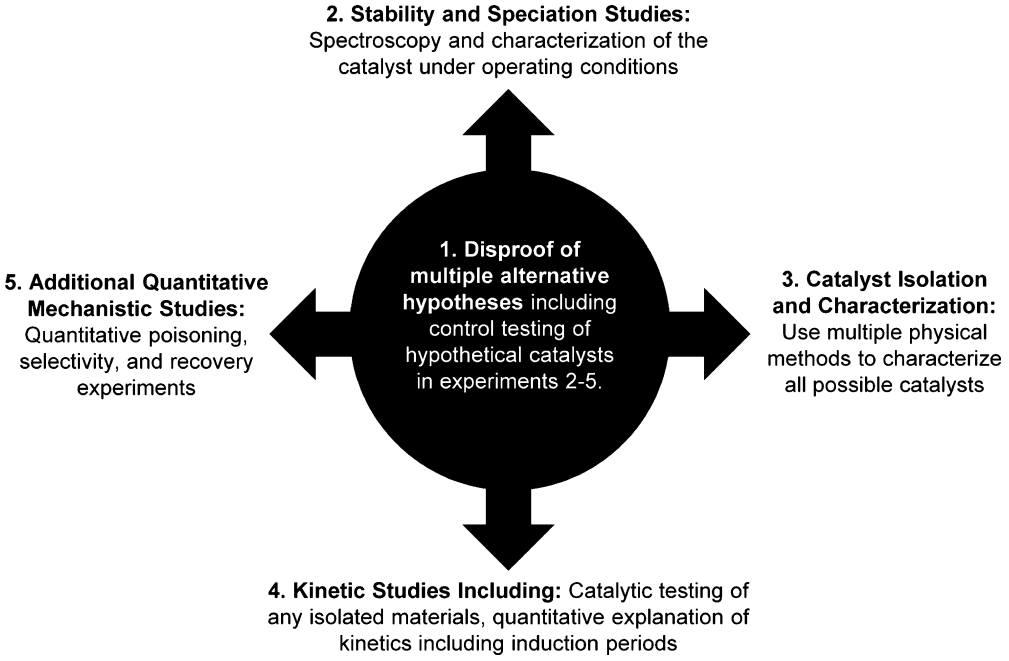

Figure 1. General methodology for distinguishing homogeneous from heterogeneous catalysts, including water oxidation catalysts. This is an updated version of the method which has been developed by our group[3,5] for identifying the true catalyst in other reactions.

true catalyst. (ii) Organic ligands decompose under the highly oxidizing conditions. And, (iii) multiple techniques are needed to characterize the catalysts. Overall, these reviews cover some of the methods and literature relevant to determining the true WOC.[6,7]

One primary, current hypothesis for overcoming the instability of organic ligands under oxidizing conditions is to use non-oxidizable complexes such as polyoxometalates (POMs).[38−41] This class of compounds, which were first synthesized in 1826,[42] possesses many properties desirable in oxidation catalysis,[43−49] namely, oxidative stability and the ability to adopt a wide variety of structures while incorporating single or multimetallic catalytic centers. The synthetic and structural aspects of this broad class of compounds has been extensively reviewed by others and will, therefore, not be addressed directly herein.[50−54] Additionally, these compounds can sometimes act as discrete metal-oxide mimics[55,56] and are therefore relevant to the study of both homogeneous and heterogeneous WOCs.

The scope of the current review is to comprehensively address the question of distinguishing homogeneous and heterogeneous water oxidation catalysis when beginning with discrete polyoxometalate precursors. This review will address the methodology and characterization methods needed to fully answer this question, describe how this methodology has been applied to the polyoxometalate WOC literature, and discuss how these results fit into the broader field of homogeneous WOCs. Note, the terms "homogeneous" and "heterogeneous" are used throughout to indicate the type of active site, as first proposed by Schwartz, and *not the phase* of the catalyst;[57] that is, a homogeneous catalyst contains a single type of active site, whereas a heterogeneous catalyst has multiple types of active sites. For example, heterogeneous metal-oxide catalysts can either be insoluble or soluble/colloidal.

An alternative nomenclature of "homotopic" and "heterotopic" has been proposed by Crabtree to indicate the type of active site.[2] Hence, for the purposes of this review, "homogeneous" means "homotopic", and "heterogeneous" means "heterotopic". Although the present review focuses on polyoxometalate WOC precursors, the general methodology for distinguishing homogeneous and heterogeneous catalysis, which has been developed in our lab for over 20 years,[3,5] is applicable to all WOCs as well as other catalytic transformations. That is, the methods and discussions which follow, for determining the true catalysts, have proved to be broadly applicable.

2. METHODS FOR DISTINGUISHING HOMOGENEOUS AND HETEROGENEOUS WATER OXIDATION CATALYSTS

The methodology to distinguish homogeneous and heterogeneous catalysts developed previously[3,5] is given in Figure 1. Rigorous identification of the true catalyst via this method consists of five basic steps: (1) generation of all possible hypotheses for the true catalyst, (2) determination of the stability of the precursor *and its speciation* ideally in operando (i.e., under the operating conditions), (3) characterization of all detectable forms of the (pre)catalyst where possible, (4) measurement of the kinetics of the reaction including controls with alternative precatalysts, and (5) conducting additional quantitative mechanistic tests, controls, and so on as required. Lastly, one must use the data in steps 2−5 to rule out all alternative forms of the catalyst en route to a final conclusion of either homogeneous or heterogeneous catalysis. Ultimately, this method is as simple or as difficult as *(i) determining where the mass of the precursor lies under the* reaction *conditions (i.e., in operando) and then (ii) quantifying the kinetic contribution of those possible catalyst forms to the observed activity.*

2.1. Generation of Hypotheses for the True Catalyst.

The central intellectual tool for identification of the active WOC is the disproof of multiple alternative hypotheses. This method, described by Platt[58] and which dates back to Chamberlain's classic 1890 paper,[59] emphasizes the need to consider any and all reasonable explanations for experimental data. In the present case of WOCs starting from POMs, the three primary competing hypotheses are (1) that the catalyst is the starting discrete

dx.doi.org/10.1021/cs4011716 | ACS Catal. 2014, 4, 909−933

polyoxometalate precursor, (2) that the POM precursor transforms into a heterogeneous catalyst such as the corresponding metal oxide, or (3) that an unknown, possibly insidious, material is the catalyst (e.g., insidious Co^{2+} as a countercation in a cobalt POM, where cobalt(II) should only be within the POM structure). It is also possible that the true catalyst is some combination of these three hypotheses—or another, presently unconceived hypothesis for the true catalyst.

Proper application of Platt's method requires careful experimental design of control experiments. These control experiments are crucial to ruling out alternative hypotheses and/or determining the limits of particular methods employed. In particular, control experiments are needed when investigating the reaction kinetics because different catalysts will, by definition, have different mechanisms. A caveat here is that one must know what the alternative catalytic material might be in order to run the correct control experiment.[3] Overall, rigorously distinguishing homogeneous and heterogeneous WOCs must rely on a method which directly attempts to disprove any alternative forms of the catalytic species in each step of the process. The following sections address these steps and the specific methods which can be applied to these catalyst identification problems with POM starting materials. Unfortunately, we will see that too often in the literature, a disproof-based method is not employed.

2.2. In Operando and In Situ Stability and Speciation Studies. A first step in identifying the true WOC is determining the stability and speciation of the precursor under the reaction conditions. Although characterization of the fate of the (pre)catalyst may seem obvious, it is frequently a challenging task due to the low precatalyst concentrations (frequently in the low micromolar range for POMs) and hence, the even lower possible concentrations of hypothetical alternative catalysts derived from the precatalyst. Polyoxometalates have the additional complication of ion-pairing with cations or limited solubility under many reaction conditions; because these complexes have large anionic charges, they interact strongly with cations derived from their precursor salts, the electrolyte/buffer, and especially polycations which sometimes include the oxidant (e.g., $Ru(bpy)_3^{3+}$). To combat these difficulties, a variety of techniques are often needed to discover the speciation of POMs under the reaction conditions. It should be noted here that although in operando characterization is best,[60,61] in operando spectroscopic methods have not yet been applied to any POM under the standard reaction conditions employed. Instead, characterization typically takes place under conditions which are in situ but take place either before or after the reaction. Hence, the use of in operando spectroscopies with POM and other WOCs is an important area for future studies.

2.2.1. UV–Vis Spectroscopy. UV–vis spectroscopy can be a useful initial method for determining the stability of polyoxometalates. Contant has used UV–vis spectroscopy to measure the association constants for numerous metal-substituted, lacunary POMs.[62,63] Only one example exists in the literature where UV–vis spectroscopy has been used to characterize a POM derived catalyst under the presence of excess oxidant.[64] Others, ourselves included, have used the visible absorption bands to measure the solution stability of POMs in situ (but, again, not precisely nor truly in operando).[65−78] For these experiments, the identity of the incorporated metal largely determines the utility of this method. For example, most cobalt-POMs have relatively weak d-d transitions in the visible region, thereby making this method useful only at high (usually millimolar) POM concentrations, as done by Galán-Mascarós in electrochemical studies where the loss in $\{Co_9(H_2O)_6(OH)_3(HPO_4)_2(PW_9O_{34})_3\}^{16-}$ was determined after bulk electrolysis.[79] In comparison, absorption coefficients of ruthenium POMs are larger,[69−73] allowing them to be measured accurately using conditions more relevant to catalysis.

POMs also have strong absorption bands in the UV region. These bands are broad and occur in all POMs and, therefore, are not a definitive characterization method. However, the large absorption coefficients for these bands have been useful in quantifying POMs which have been separated by HPLC (vide infra),[80] as was done to determine the oxidative stability of $[Co_4(H_2O)_2(PW_9O_{34})_2]^{10-}$ at ∼1.25−5.0 μM concentrations.[81]

2.2.2. Electrochemistry. Polyoxometalates have a rich electrochemistry associated with both reduction of tungsten or molybdenum and oxidation of heteroatoms (i.e., the incorporated cobalt, ruthenium, iridium, or nickel heterometal atoms, metals of special interest for WOCs[13,16,17]). These characteristic peaks can be used to identify POMs, especially when used in conjunction with other physical methods. Electrochemical methods can also be used to characterize possible intermediates in the water oxidation reaction, as is common for ruthenium-based POMs.[82−84] In addition to direct measurements of the POMs, electrochemical methods have also been used to quantify decomposition products, including aqueous Co^{2+}, and CoO_x or MnO_y films which form under oxidizing conditions.[66,81,85−89] This ability to electrodeposit metal-oxide films, if present, is advantageous, because it allows one to easily isolate and then characterize these films, which are often very active WOCs.[19,66,79,81]

Conversely, the electrode can make it difficult to identify homogeneous catalysts, because electrodeposition of heterogeneous metal oxides will concentrate and enhance the effect of any metal-oxide film over relatively dilute solution species, thereby obscuring any homogeneous activity. Note, however, that this concentrating effect can also be observed for any adsorbed, anionic material, including adsorbed polyoxometalates on a positively polarized electrode.[90−92] This phenomenon has been followed by electrochemical quartz crystal microbalance studies for water oxidation studies starting with $[(Mn(III)(H_2O))_3(SbW_9O_{33})_2]^{9-}$.[87] In our own studies, we also have electrochemical evidence that $[Co_4(H_2O)_2(PW_9O_{34})_2]^{10-}$ may be adsorbing to glassy carbon electrodes in both pH 5.8 and 8.0 sodium phosphate solutions.[81] One caveat in electrochemical studies is that sometimes the redox activity of transition-metal-substituted POMs is absent, depending on the specific POM, the electrode material, or the pH, thereby making electrochemical methods useful in only some cases.

One electrochemical method which has found wide use in studies of WOCs is the measurement of a current-overpotential[93] relationship. In this method, the log of the current is plotted versus the log of the overpotential, which results in a straight line for well-behaved systems; this is also known as a Tafel plot.[94] The slope of the fitted line is ultimately related to the catalytic mechanism. For example, a slope of 60 mV/decade (i.e., the current changes by an order of magnitude when the overpotential is increased by 60 mV) is consistent with a reversible one-electron transfer followed by a chemically turnover-limiting step, whereas a 120 mV/decade slope could be consistent with a turnover-limiting electron transfer step. Others have used these plots as a qualitative method to differentiate between catalysts. Additional discussion of current−overpotential relationships can be found elsewhere.[94]

dx.doi.org/10.1021/cs4011716 | ACS Catal. 2014, 4, 909−933

In short, electrochemical methods allow one to both measure catalyst activity as a function of driving force and characterize redox active reaction intermediates and their stability en route to identifying the true WOC.

2.2.3. NMR/EPR. Because POMs typically have no organic ligands (unless intentionally functionalized), NMR characterization typically relies on ^{31}P, ^{183}W, ^{51}V, ^{95} Mo, and ^{17}O nuclei, the last of which must be intentionally incorporated in most applications.[95−97] A primary benefit of NMR, is that it can directly follow the stability and speciation of POMs, because the number and chemical shift of peaks are often definitive fingerprints for POMs. For example Contant and Zhu et al. have used NMR (among other methods) to study the pH-dependent speciation of phosphotungstates.[98,99] Despite the utility of NMR spectroscopy, it has been used relatively infrequently for POM WOC studies since many of the species are paramagnetic, thereby broadening and shifting peaks while requiring higher catalyst concentrations for detection.[100] However, Hill and co-workers have successfully used ^{31}P NMR to qualitatively demonstrate the presence of a $[Co_4(H_2O)_2(PW_9O_{34})_2]^{10-}$ species at the end of water oxidation reactions using a $Ru(bpy)_3^{3+}$ oxidant.[65] In other, noncatalytic studies, Ohlin et al. have used ^{17}O NMR to measure the rate of water ligand exchange on $[Co_4(H_2O)_2(PW_9O_{34})_2]^{10-}$ and found a fast 1.5×10^6 s^{-1} water exchange rate constant—a necessary requirement for highly active WOCs.[101] Overall, NMR is potentially useful in quantifying POM stability under reaction conditions, but the technique has found limited application due to low magnetic receptivity of ^{183}W and ^{95}Mo, solubility issues (vide infra), and the presence of paramagnetic metal centers.

The presence of paramagnetic redox centers open up the possibility of EPR spectroscopic characterization. Ruthenium POMs have been characterized by EPR including, $[Ru_4(\mu\text{-}O)_4(\mu\text{-}OH)_2(H_2O)_4(\gamma\text{-}SiW_{10}O_{36})_2]^{10-}$ and $[Ru(H_2O)SiW_{11}O_{39}]^{5-}$ and their higher oxidation state analogues.[64,76] EPR has also been used to determine the solution stability of $[Co_4(H_2O)_2(PW_9O_{34})_2]^{10-}$ and $[Co_4(H_2O)_2(P_2W_{15}O_{56})_2]^{16-}$, where aqueous, leached Co^{2+} is also EPR active.[101] Although this method can illuminate possible paramagnetic solution species, kinetic studies are needed to connect the observed species to water oxidation activity.

2.2.4. IR, Raman, and Resonance Raman. Due to the large number of vibrational bands, IR spectra are often used as diagnostic fingerprints. In general, IR characterization is used to either identify a particular compound or to verify the presence of the hypothesized catalyst after it has been isolated from the postreaction solution.[65,69,72,78,79,102] However, since water interferes with collection of IR, this method is generally not applicable to in situ or in operando characterization of water oxidation catalysts.

Raman and resonance Raman (rRaman) have proven to be more useful than IR when characterizing POMs under water oxidation reaction conditions.[103] Resonance Raman is especially useful since it allows the catalyst/precatalyst to be selectively excited, thereby enhancing the signal-to-noise ratio and allowing lower concentrations of catalyst to be investigated. This method has been used to investigate the reaction intermediates in ruthenium WOCs where the conversion of Ru−OH_2 into Ru=O bonds occurs upon oxidation.[64,76] Regions of particular relevance to water oxidation catalysis are the M−OH and M−OH_2, which appear from 330 to 550 cm^{-1} for $[Ru_4(\mu\text{-}O)_4(\mu\text{-}OH)_2(H_2O)_4(\gamma\text{-}SiW_{10}O_{36})_2]^{10-}$ (and its oxidized products) and the M = O at ∼800 cm^{-1} for $[Ru(O)SiW_{11}O_{39}]^{5-}$.[64,76] The strength of Raman spectroscopy ultimately derives from its potential ability to characterize WOCs in operando and is a potentially powerful, underutilized method at present.

2.2.5. EXAFS/XANES. Extended X-ray absorption fine structure (EXAFS) and X-ray absorption near edge structure (XANES) are valuable techniques to probe both the local coordination environment and the oxidation state of either solution or solid-state materials. Despite the potentially powerful nature of these experiments, characterization of $[Ru_4(\mu\text{-}O)_4(\mu\text{-}OH)_2(H_2O)_4(\gamma\text{-}SiW_{10}O_{36})_2]^{10-}$ reaction intermediates is presently the only example of EXAFS/XANES in the POM WOC literature.[104] Unfortunately, in the case of $[Ru_4(\mu\text{-}O)_4(\mu\text{-}OH)_2(H_2O)_4(\gamma\text{-}SiW_{10}O_{36})_2]^{10-}$, the ruthenium EXAFS/XANES is nearly identical to a heterogeneous RuO_2 material, thereby obfuscating the ability to distinguish a homogeneous versus heterogeneous catalyst during catalytic water oxidation (which was not pursued in this example;[104] prior evidence is consistent with a homogeneous POM catalyst[72]). In addition, the optimum use of these X-ray absorption methods requires accurate models which may or may not be available for hypothetical heterogeneous MO_x WOCs. Pure materials or knowledge of the catalyst speciation is also needed since EXAFS is a bulk technique which measures the average absorption. Therefore, EXAFS/XANES provide strong evidence for the active catalyst under the reaction conditions but only if the speciation and kinetics have been measured by other techniques.

2.2.6. Dynamic Light Scattering and Small Angle X-ray Scattering. This last set of characterization techniques, namely, dynamic light scattering (DLS) and small-angle X-ray scattering (SAXS), are aimed at determining whether particles are formed in solutions and, if present, their size. Of these methods, DLS has found the broadest usage due to the wide availability and the ability to measure particles in situ.[68,74,78,105,106] Throughout the POM WOC literature, the putative absence of particles in a postreaction solution has been used as evidence to rule out heterogeneous WOCs. However, this conclusion follows only if the underlying assumption, that all heterogeneous materials can be detected, is true—a potentially difficult analytical problem since the sensitivity of DLS decreases with the particle radius and concentration.[107,108] That is, the lack of observed particles only guarantees that there are no particles *above the detection limit of the method*, not that lower concentrations of potentially very catalytically active particles are not there. Conversely, the presence of particles does not guarantee a heterogeneous metal-oxide material is the catalyst since POMs can also precipitate under the reaction conditions, especially when cationic oxidants such as $Ru(bpy)_3^{3+}$ are used.[65,69,70] In summary of DLS and SAXS methodology in the WOC area, these methods can provide evidence for particles, in which case additional experiments are needed to characterize these materials and demonstrate the catalytic kinetic competence (or not) of the particles. Additionally, when no particles are observed, controls are critical to determining the detection limit of these methods in order to rule out (or support) the possibility of highly active, heterogeneous WOCs.

2.3. Catalyst Isolation and Ex Situ Characterization, Where Possible. Once the speciation of the POM starting material is known, a third, useful step in distinguishing homogeneous and heterogeneous catalysis is isolation and ex situ characterization of any detected forms of the catalyst. This step is closely tied to the second since it involves determining where the catalyst mass lies and its precise composition. However, caution must be taken when interpreting ex situ characterization results since isolation processes can alter the material. In addition, ex situ methods also tend to be more qualitative and overall less definitive

dx.doi.org/10.1021/cs4011716 | ACS Catal. 2014, 4, 909−933

than in operando methods. IR and NMR are often utilized on the resultant isolated materials, but these methods have already been addressed (sections 2.2.3 and 2.2.4, vide supra) and, therefore, will not be discussed further here. Because isolation of POM or heterogeneous MO_x materials is required prior to any ex situ characterization, isolation methods that have proven useful are provided first in what follows.

2.3.1. Extraction. Due to the large anionic charge of most POMs, they interact strongly with a variety of organic solvent soluble cations such as tetra-alkyl ammoniums. Strong cation^{m+}-POM^{n-} interactions allow one to extract POMs from aqueous solutions into organic solvents which contain alkyl-ammonium cations.[109] In addition to isolation of the POM, an extraction can leave behind cationic decomposition products. Hill and coworkers elegantly leveraged this technique to determine the hydrolytic stability of $[Co_4(H_2O)_2(PW_9O_{34})_2]^{10-}$; the POM was extracted from aqueous solution using toluene/tetra-*n*-heptylammonium nitrate, and then the remaining aqueous Co^{2+} was quantified by ICP-MS.[67] One complicating factor of extraction is that although the POM has been separated from the aqueous solution, additional isolation methods, such as recrystallization, are needed to recover the POM from the organic solvent.

2.3.2. Precipitation/Filtration/Centrifugation. Perhaps the easiest way to isolate POMs from solution is via precipitation upon addition of an excess of cations.[65,68,69,72,79] For this purpose, large cations such as Cs^+ or $Ru(bpy)_3^{2+}$ are most effective due to size-matching effects resulting in high solid-lattice energies. Indeed, when chemical/photochemical oxidants are used to drive the water oxidation reaction, POMs often precipitate prior to or during the reaction (a factor which also complicates the observed kinetics as discussed in section 2.4). Once the POM has been precipitated, it can easily be collected by filtration or centrifugation. The filtrate or supernatant can also be tested for residual catalytic activity to help determine the phase of the catalyst.

2.3.3. HPLC. Separation of multiple POM or other species is difficult to achieve if the species possess similar solubility, charge, and/or size characteristics. One of the few methods capable of this separation is reverse-phase, ion-pair HPLC where the combination of (alkyl-cation)-POM plus (alkyl-stationary-phase)-(alkyl-cation) interactions allow POMs to be separated based primarily on their charge.[80] Application of this HPLC method has allowed the stability of $[Co_4(H_2O)_2(PW_9O_{34})_2]^{10-}$ to be quantified using postelectrocatalytic reaction solutions.[81] Controls using pre-established UV−vis extinction coefficients are also useful to verify whether or not the POM of interest is soluble in the eluting solvents and is stable on the column.[80,81] Two limitations of this method are that MO_x materials have not yet been successfully separated by HPLC, and precipitated POM materials will not be observable. Overall, in favorable cases HPLC can put a lower limit on the POM stability, but it is an indirect method where controls plus caution are needed in interpreting the results, especially since conditions on the HPLC column are typically far different than the catalytic conditions. Also, HPLC is, in our experience, not able to identify where any missing (pre)catalyst mass lies.

2.3.4. Electrodeposition/Electrode Rinsing. When a positively biased electrode is the oxidant source, the electrode material can easily be removed from the polyoxometalate solution and rinsed with water to remove residual electrolyte or soluble catalyst.[66,79,81] The resultant electrode can then be subjected to a battery of tests to characterize its surface; it can also be placed in POM-free solution and tested for residual catalytic activity. This simple experiment can be very telling if a heterogeneous metal-oxide catalyst is present on the electrode surface and especially if that solid oxide is the dominant WOC. However, caution should be exercised when interpreting these rinsing experiments since some MO_x catalysts are not stable under the highly oxidizing conditions needed for water oxidation—CoO_x instability at 1.4 V versus Ag/AgCl in pH 8 sodium phosphate is a case in point.[81] A variety of POMs, including Co or Mo containing POMs, are known to adsorb strongly to glassy carbon and mercury electrodes.[81,87,90−92] Hence, a significant caveat here is that the absence of a metal-oxide film cannot rule out heterogeneous catalysis, and residual activity after rinsing cannot definitively rule out homogeneous POM catalysis.

2.3.5. Postelectrolysis Surface Characterization (SEM, EDX, WDS, XPS). To visualize and characterize an electrode used for electrochemically driven water oxidation, scanning electron microscopy (SEM) with energy dispersive X-ray spectroscopy (EDX) (or wavelength dispersive X-ray spectroscopy, WDS) analysis is a useful first step.[66,79,81,110] This technique requires that a catalytically active material remains on the electrode surface. When a deposited catalyst is present, EDX or WDS can provide qualitative identification of, and ratios for, the elemental components of the material. This information can then be used to provide evidence for or against the starting POM being deposited on the electrode, within the detection limit of the method.[111] However, care should be taken in interpreting these results since the high energy (∼5−15 keV) incident electron beam, which ultimately results in the element specific X-ray emission, penetrates to depths of micrometers and therefore is relatively surface insensitive.[111] For nanometer thick films or monolayer coverage of electrodes, surface-sensitive techniques are more appropriate.

X-ray photoelectron spectroscopy (XPS) is one technique which is more surface sensitive than EDX but which provides similar information on the elemental makeup of a postelectrolysis electrode.[81] Because this technique relies on the detection of relatively low-energy (<1 keV) emitted electrons, only the surface 1−20 nm allows a significant portion of these electrons to escape.[112] XPS has the benefit of providing additional characterization data since the measured binding energy (i.e., the energy of the ejected electrons) depends on the oxidation state and chemical environment of each element. Controls examining known materials are therefore powerful in distinguishing between different materials/compounds, even when the same elements are present (e.g., distinguishing between Co_3O_4 and CoO). Overall, ex situ characterization of postreaction electrodes can lead to critical information when a catalytic material remains deposited or adsorbed. That said, the lack of a detectable catalytic material provides little insight into the true WOC.

2.3.6. TEM. Technological advancement and broadening availability of transmission electron microscopy (TEM) has led to the widespread use of this primarily ex situ method in visualizing nanometer and subnanometer particles which can form during water oxidation reactions.[113] Unlike SEM, which is primarily for analysis of electrochemically driven reactions, TEM can be used to analyze the postreaction solution components regardless of the oxidant source. As noted in our 2003 review on distinguishing homogeneous from heterogeneous catalysts,[3] several limitations of TEM should be considered when using ex situ microscopy evidence in support of a homogeneous versus a heterogeneous catalyst hypothesis. First, TEM does not provide direct evidence for catalysts, but rather indicates the

dx.doi.org/10.1021/cs4011716 | ACS Catal. 2014, 4, 909−933

presence or absence of materials which *might* be catalysts; stoichiometry (i.e., how much of the starting material is converted into possible catalytic materials under, ideally, in operando conditions) *and kinetics* are needed to provide supporting evidence for the true catalyst. Second, beam damage can occur when using electron microscopy, where nanoparticles are formed within the electron beam.[114] Controls are therefore needed to verify the stability of starting materials under the beam.[114] Third, most water oxidation systems (and POMs in particular) have the added difficulty of a low concentration of precatalyst in the presence of a very large excess of nonvolatile buffer (e.g., a precatalyst:buffer ratio of up to 1:10^4).[67] That is, finding and detecting the presence of nanoparticle catalysts (if they are present) can become exceedingly difficult under such dilute conditions. Therefore, if TEM is invoked as evidence against a heterogeneous catalyst, one should also demonstrate that *control experiments can easily detect the amount of heterogeneous material needed to account for the observed catalytic activity*. Due to the limitations noted above, TEM has been used much less frequently in identifying heterogeneous WOCs than in metal(0) nanoparticle literature where reducing conditions are typically used.[3]

2.3.7. MS and ICP/MS. Mass spectrometry (MS) is another characterization method which lends itself to both speciation (section 2.2) and ex situ characterization (section 2.3) studies; MS is classified as the latter, ex situ method for the purposes of this review. To our knowledge, MS has not yet been used to characterize POMs under catalysis conditions, even though MS can provide very strong evidence for the presence of specific species due to the high molecular weights and characteristic isotopic peak ratios, as reviewed by Cronin and co-workers.[115] Of course, MS has the disadvantage that only species which can be desorbed/ionized into the gas phase will be observed. Hence, only with extensive controls on authentic, possible heterogeneous and other catalysts can MS accurately report on the presence, or absence, of catalytic materials.

However, POMs do lend themselves to tandem isolation-ICP/MS (inductively couple plasma-MS) methods which can be used to infer the solution speciation. For example, Hill and co-workers have used POM-extraction plus ICP/MS of the resultant aqueous solution to quantify the dissociation of Co^{2+} from a $[Co_4(H_2O)_2(PW_9O_{34})_2]^{10-}$ starting material.[67] Others have used HPLC/ICP/MS (in conjunction with ^{31}P NMR) to determine the speciation of phosphotungstates as a function of pH (although these POMs were not studied for their catalytic activity).[99] Hence, MS and ICP/MS can provide speciation and characterization data which are complementary to in situ spectroscopies such as NMR, Raman, X-ray absorption, and UV−vis. Although isolation and ex situ characterization is, again, less desirable than in operando characterization due to the possibility of sample alteration during the experiment, all of the ex situ methods described in the above section (3.3) can provide visual and elemental analysis evidence necessary for correct identification of possible catalytic species.

2.4. Kinetics. Distinguishing homogeneous and heterogeneous WOCs *requires* kinetic studies since, in the words of Jack Halpern, "catalysis is, by definition, purely a kinetic phenomenon".[116] Every catalyst has a characteristic mechanism which determines the observed kinetics. Therefore, understanding the kinetic dependence of the reaction variables is absolutely required for unequivocal identification of the true catalyst.

Dioxygen (O_2) evolution kinetics are one of the most relevant metrics, since the desired product of $4e^-$ water oxidation is O_2 (and $4H^+$). Oxygen evolution can be measured using several different methods, including electrochemically (e.g., a Clark-type electrode), fluorescence quenching probes, gas chromatography, or a pressure transducer, the latter along with independent verification that O_2 is in fact the gaseous product being measured.[72,74,76,81,117−119] Alternatively, one can measure oxidant consumption[120] or oxidation current as a *proxy* for O_2 evolution, if the overall efficiency for the reaction is near 100%. However, one must verify that the oxidant is being quantitatively used for the O_2 evolution reaction in order to be able to correlate the rate of oxidant loss directly to the rate of O_2 evolution (the latter divided by the stoichiometric factor of 4, i.e., $-d[1e^-\text{ oxidant}]/dt = 4\, d[O_2]/dt$). This point is especially relevant since stoichiometric conversion of the oxidant into O_2 is rarely observed, because side-reactions are possible, notably 2,2′-bipyridine ligand oxidation when $Ru(bpy)_3^{3+}$ is used as the oxidant.[121,122] When a chemical oxidant is used the efficiency is usually referred to as the "O_2 yield", whereas when electrochemical oxidation is used the term "faradaic efficiency" is most common. In general, faradaic efficiencies tend to be higher than chemically driven O_2 yields conducted under otherwise similar conditions since fewer side oxidation reactions seem to be observed, at least to date, when electrochemical oxidation is used.

An additional complicating factor observed in O_2 evolution kinetics is the presence of sigmoidal or S-shaped kinetic curves. Sigmoidal curves and other curves with induction periods have been observed in the literature when the starting material is converted into a more active catalytic material (i.e., when the starting material is not the catalyst and is converted into a heterogeneous catalyst).[3] Increasing catalytic activity with time is *prima facie* evidence that the starting material is not the best catalytic material—and, hence, an indication that additional characterization (ideally in operando) is needed to determine the actual catalyst that is being formed.

However, the other possible explanation for sigmoidal kinetics is that the S-shape is only an artifact and is caused by (1) a slow response time for the O_2 quantification method, or (2) slow solution-to-gas mass transfer when the method samples the reaction vessel headspace. Both of these complications are likely prevalent in the WOC literature since solution-based probes often have response times of 8−30 s (e.g., the widely used FOXY or commercially available Clark electrodes),[81,117] and since pressure transducers and GC methods rely on headspace analysis. Hence, faster, reliable O_2 quantification methods will be needed to study and understand the increasingly active homogeneous and heterogeneous WOCs currently being developed.

2.4.1. Controls. Kinetic controls are a critical experiment type for accurate identification of the true WOC. As noted above, the catalytic mechanism is ultimately played out, and leaves its most definitive fingerprint, in the kinetics. Therefore, one can provide strong evidence for or against a homogeneous POM WOC by comparing the kinetics of the POM *to the kinetics of heterogeneous WOCs*.[67,76,84,123,124] For example, Hill and co-workers tested the activity of $RuCl_3$ and RuO_2 en route to concluding that $[Ru_4(\mu\text{-}O)_4(\mu\text{-}OH)_2(H_2O)_4(\gamma\text{-}SiW_{10}O_{36})_2]^{10-}$ is a WOC.[119] Galán-Mascarós and co-workers have used $Co^{2+}$and Co_3O_4 materials in efforts to distinguish $\{Co_9(H_2O)_6(OH)_3(HPO_4)_2(PW_9O_{34})_3\}^{16-}$ and CoO_x catalysts.[102] We used Co^{2+} and CoO_x controls to determine the relative stability and activity of these precursors compared to $[Co_4(H_2O)_2(PW_9O_{34})_2]^{10-}$.[81] The caveat to all of these control studies is that the precise catalyst may not be known, and it therefore may not be possible to conduct the best,

dx.doi.org/10.1021/cs4011716 | ACS Catal. 2014, 4, 909−933

most telling control experiments. Also, if a heterogeneous catalyst is being tested, the number of active sites needs to be taken into account but is typically not known and often difficult to determine. In short, the full rate law, plus several controls with multiple precursors, are necessary to provide compelling kinetic evidence for (or against) the final conclusion of a homogeneous (or heterogeneous) WOC.

2.5. Phenomenological Studies: Ligand or Poison Additions. The last set of experiments for distinguishing homogeneous and heterogeneous WOCs involves additional, ideally quantitative mechanistic tests. These experiments involving the addition of exogeneous ligands or poisons are often basically kinetic experiments, although as presently performed they are frequently more qualitative in nature—despite the fact that *quantitative poisoning studies can be one of the single most powerful means to distinguish homogeneous from heterogeneous catalysts.*[125] For example, Hill and co-workers[65] and Goberna-Ferrón et al.[79] removed excess aqueous Co^{2+} by adding 2,2′-bipyridine (bpy) to their $[Co_4(H_2O)_2(PW_9O_{34})_2]^{10-}$ and $\{Co_9(H_2O)_6(OH)_3(HPO_4)_2(PW_9O_{34})_3\}^{16-}$ solutions, respectively; the authors conclude that the remaining water oxidation activity is therefore due to the starting POM since controls with Co^{2+} plus 2,2′-bipyridine show no O_2 evolution activity. Although this bpy addition experiment argues against a Co^{2+} to CoO_x catalyst formation pathway, one must also know the stability of the POM under the reaction conditions to rule out a POM to CoO_x WOC formation pathway. Other phenomenological tests include addition of different counter cations and anions, changes in buffer, and changes in oxidant; as with bpy addition, changing any one of these variables might provide insight into the active catalyst, *or* it could potentially change the true catalyst identity.

As noted above, *quantitative* poisoning studies can be very telling—and sometimes *the* definitive piece of distinguishing evidence—in studies of homogeneous versus heterogeneous catalysts.[2,3,125] The missing piece here at present, however, is a general water oxidation catalyst poison, one that is both an effective poison and is also stable to WOC oxidation potentials.

2.6. Summary of the Methodology. The methodology described herein is meant as a general guide to the reader as well as a practical guide for the practitioner. As with many areas of chemical science, the ability to identify the true WOC will continue to evolve as analytical methods are improved. Overall, the problem of distinguishing homogeneous and heterogeneous catalysis is as simple or as complex as (i) identifying any and all possible catalytic materials, and then (ii) obtaining the catalytic water oxidation activity (and rate laws) of those observed materials and comparing and correlating that data with the observed water oxidation reaction kinetics.

The next section will describe specific studies of water oxidation catalysis when beginning with POM starting materials and the experiments reported therein to distinguish homogeneous and heterogeneous catalysis.

3. WATER OXIDATION CATALYSIS STUDIES BEGINNING WITH POLYOXOMETALATES

Presently, there are 38 literature examples of water oxidation catalysis studies which use 28 different polyoxometalates as the starting materials. These reports include cobalt-, ruthenium-, manganese-, molybdenum-, iridium-, and nickel-based POMs, in order of decreasing prevalence. The following sections are separated according to the (hypothetically) active metal center. Each metal is then divided into two subsections: (1) precedent in terms of examples of non-POM studies with that metal which provide evidence for conversion of homogeneous starting materials into heterogeneous WOCs, and then (2) WOC studies which start with polyoxometalates containing that same metal. The first subsection is needed to put the POM studies into broader perspective within the WOC literature as well as to suggest metal-specific experiments which have been used successfully to distinguish homogeneous and heterogeneous WOCs. The second subsection for each metal then addresses the specific studies of POMs while critically analyzing the experimental data relevant to identifying the true catalyst. Note that the term "precatalyst" is used throughout this section to indicate the species which is present prior to the reaction, whereas the term "catalyst" is reserved for the species present in the catalytic cycle and can, for example, be either homogeneous or heterogeneous.

3.1. Cobalt. *3.1.1. Non-POM Cobalt Precatalysts.* Determining the true catalyst in cobalt-based water oxidation systems has been addressed beginning with some of the earliest studies which used cobalt(II) salts as starting materials. In these cases, distinguishing homogeneous and heterogeneous catalysis has proved to be challenging in part due to the possible formation of potentially low amounts of hard-to-detect, ostensibly high-activity, colloidal CoO_x. Despite these difficulties, Parmon and co-workers have made significant progress on this problem, starting back as early as 1981, by studying both homogeneous cobalt precursors (e.g., $CoCl_2$) and heterogeneous colloidal cobalt(III) hydroxide in the presence of chemical oxidants (e.g $Ru(bpy)_3^{3+}$).[126−133] Ultimately, they concluded that the true catalyst is the same when beginning with either aqueous cobalt salts or heterogeneous cobalt(III) hydroxide since the catalytic O_2 generation rate and yields are identical for both starting materials, even when the conditions are varied (e.g., the pH, the catalyst-to-oxidant ratio, and when additional cations are provided).[131]

More recently, Shevchenko et al. reported in 2011 that aqueous cobalt $[Co(ClO_4)_2]$ plus methylenediphosphonate solutions will transform into catalytically active CoO_x colloidal solutions using photochemical ($h\nu$ + $Ru(bpy)_3^{2+}$ + $Na_2S_2O_8$) or chemical ($Ru(bpy)_3^{3+}$) oxidants.[134,135] Interestingly, by including or excluding the methylenediphosphonate, the authors were able to control the size of the CoO_x colloids (10−60 nm in the presence of and 50−2500 nm in the absence of methylenediphosphonate), thereby exhibiting some control over the catalytic activity of the colloids. Shevchenko et al.'s paper is of additional importance in that it provides evidence consistent with the existence of anion-stabilized CoO_x colloids—a possibility which is not addressed in the current POM WOC literature.

In a related study, Fukuzumi and co-workers have investigated CoO_x WOCs derived from homogeneous cobalt precursors such as $[Co(Cp^*)(bpy)(OH_2)]^{2+}$ and $[Co(tris(N,N'$-dimethylaminoethyl)-amine$)(OH_2)]^{2+}$.[136] When these precursors were illuminated in the presence of $Ru(bpy)_3^{2+}$ and $Na_2S_2O_8$, the formation of 20 ± 10 nm and 200 ± 100 nm particles were observed by dynamic light scattering and TEM. The resultant O_2 evolution total turnovers (TTO) was also measured and is higher for the smaller versus larger particles, 420 versus 320 mols O_2/mols Co, respectively. The authors conclude that organic ligands appear to stabilize in situ formed CoO_x particles during photodriven water oxidation, but neither direct evidence for CoO_x-ligand bonds nor the Co/ligand ratio(s) involved was provided.

Water oxidation catalysis when beginning with cobalt salts and electrochemical oxidation has been studied as well.[137] Although several papers reported that aqueous Co(II) solutions form a

dx.doi.org/10.1021/cs4011716 | ACS Catal. 2014, 4, 909−933

heterogeneous cobalt−oxy−hydroxy material, the activity of these in situ formed oxides was not studied in the presence of the Co(II) precursor until Nocera and co-workers began investigations of these systems in 2008.[138,139] Therein, Nocera and co-workers demonstrate that when aqueous Co(II) is electrolyzed above 1.05 V versus NHE in neutral to slightly basic solution, a CoO_x material forms which is composed of cobalt, oxygen, and adventitious electrolyte cations and anions.[138,139] Additional studies of CoO_x have shown that these materials are self-healing, contain cobalt in primarily the Co(III) and Co(IV) oxidation states, and are composed of cobalt−oxo cubane domains which are more or less ordered depending on the deposition conditions.[140−145]

In a related study, attempts to make a homogeneous $Co(III)F_3$ water oxidation catalyst by Gerken and Stahl also resulted in the formation of a heterogeneous CoO_x material. Under their conditions, they observed by EDX a material which consisted of Co/O/F in a ratio of 1:6:0.3.[146] In addition, by electrodepositing several different CoO_x materials (including the CoPi-type CoO_x of Nocera and co-workers, op. cit.), Gerken and Stahl showed that all of the CoO_x had similar activity and equilibrated with the reaction solution to form nearly identical materials after bulk electrolysis.

A subsequent, pivotal study by Stahl and co-workers elaborated upon their initial results by investigating aqueous Co(II) precursors from pH 1−14.[147] Therein, it was found that three pH regimes were found: (i) at pH > 5.5, stable CoO_x films were formed on the electrode; (ii) at 5.5 > pH > 3, a CoO_x film could be formed on the electrode, but it was oxidatively unstable and would dissolve during electrolysis if excess Co(II) was not present in the solution; (iii) at pH < 3, no film was observed on the electrode and the dependence of activity on aqueous Co(II) followed an adsorption isotherm—evidence which is consistent with the active catalyst precursor being the dissolved cobalt(II) species. This important study demonstrates that the stability of heterogeneous CoO_x catalysts can vary with reac tion conditions and that CoO_x films are unstable at pH < 3. Restated, the absence of an observed heterogeneous material at the *end* of a reaction does not guarantee it was not present and active *during* the reaction, depending on the pH and other conditions to start and at the end of the reaction—H^+ being a product of the oxidation of water. Furthermore, by comparing the kinetics and products of the water oxidation reaction, these authors were able to differentiate between the homogeneous and heterogeneous catalyst systems which differ only in the pH employed.

3.1.2. Cobalt POM Precatalysts. Perhaps the most intensely studied complex in the recent water oxidation literature is the cobalt polyoxometalate $[Co_4(H_2O)_2(PW_9O_{34})_2]^{10-}$ (Co_4POM) (Figure 2). This compound was first reported to be a WOC in a 2010 *Science* paper by Hill and co-workers with a high turnover frequency (TOF = 5 s^{-1}, albeit for an unknown rate law[117]) when using a $Ru(III)(bpy)_3^{3+}$ oxidant at pH 8.[65] Therein, the authors provided several experiments consistent with their hypothesis that Co_4POM is the true catalyst. First, the Co_4POM was reported to be stable by UV−vis and ^{31}P NMR spectroscopy at pH 8 over 1 month, consistent with at least some hydrolytic stability of the complex, although the claimed stability was not quantitated, nor were error bars given. Second, 2,2′-bipyridine was added to the solution in order to complex any adventitious aqueous Co(II), which would form a CoO_x catalyst in situ, if present; this caused the O_2 yield to decrease from 67% to 48% for the 3.2 μM Co_4POM solution in the absence and presence of the 2,2′-bipyridine. In contrast, controls beginning with 13 μM $Co(NO_3)_2$ showed O_2 yields of 80% and 0% when 2,2′-bipyridine was absent or present. These results suggest that at least CoO_x formed solely from aqueous Co(II) is not the dominant catalyst in the Co_4POM system.

Qualitative evidence that the Co_4POM is largely (i.e., but again, not quantitatively) stable during the reaction was demonstrated by observation of the ^{31}P NMR signal for the polyoxometalate in the postreaction solution which had been treated with sodium tetraphenylborate to precipitate $Ru(II)(bpy)_3^{2+}$. Additionally, the Co_4POM could be precipitated from the postreaction solution by addition of excess $Ru(II)(bpy)_3^{2+}$ and showed IR signals consistent with the starting POM. This precipitated $[Co_4(H_2O)_2(PW_9O_{34})_2]^{10-}$:$Ru(II)(bpy)_3^{2+}$ material was then dissolved and tested for water oxidation activity by addition of $Ru(III)(bpy)_3^{3+}$ oxidant, resulting in an O_2 yield of 49%. Although these results are all consistent with the authors' hypothesis/conclusion that the Co_4POM is the true catalyst, they did not rule out the possibility that a portion of the starting Co_4POM is transformed into either a different POM fragment or a heterogeneous CoO_x catalyst under the reaction conditions. That is, in order to rule out this possible formation of a highly active derivative material, additional studies were required.

Subsequently, Hill, Lian, and co-workers also reported the Co_4POM as a photochemically driven WOC where the oxidizing equivalents were derived from the common $Ru(II)(bpy)_3^{2+}$, Na_2SO_8, plus hν system with a maximum O_2 yield of 45%.[105] Therein, the authors reported that no evidence for particle formation was observed by dynamic light scattering and Tyndall effects under conditions of 1 mM $Ru(bpy)_3^{2+}$, 160 mM NaBi, pH 8, 5 μM Co_4POM, 5 mM $Na_2S_2O_8$. This is an interesting result since a prior report[65] by the same group said that supersaturated solutions of Co_4POM were formed when as few as 40 equivalents of $Ru(bpy)_3^{2+}$ were present (i.e., which would translate to 200 μM $Ru(bpy)_3^{2+}$ in the photochemical system). Although the absence of detectable CoO_x colloids is a relevant result, one must also know what concentration and size of CoO_x colloids would account for the observed activity and then determine whether that amount and size of colloid *can be detected* via dynamic light scattering (or any other measurement of suspended colloids).

Reinvestigation of the photochemically driven $Ru(bpy)_3^{2+}$ plus Co_4POM was conducted by Natali et al.[85] In this study, the Co_4POM was aged and then subjected to flash photolysis—an experiment wherein $Ru(III)(bpy)^{3+}$ is photochemically generated by quenching of the $Ru(II)(bpy)_3^{2+*}$ excited state by sodium persulfate and then the rate of $Ru(II)(bpy)_3^{2+}$ recovery is observed as a function of time. In these experiments, it was found that the amount of $Ru(II)(bpy)_3^{2+}$ recovered during

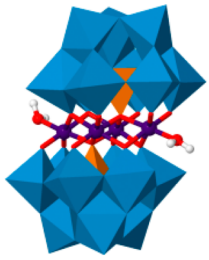

Figure 2. Mixed polyhedral/ball-and-stick model of $[Co_4(H_2O)_2(PW_9O_{34})_2]^{10-}$ where blue polyhedral = WO_6, orange polyhedral = XO_4 (X = P or Si), purple = Co, red = O, white = H.

dx.doi.org/10.1021/cs4011716 | *ACS Catal.* 2014, 4, 909−933

the first 100 μs increased with increasing Co_4POM aging time. The $Ru(II)(bpy)_3^{2+}$ recovery plateaued for Co_4POM solutions aged 90 min or more when the initial conditions were $[Ru(II)(bpy)_3^{2+}] = [Co_4POM] = 50\ \mu M$, 5 mM $Na_2S_2O_8$, pH 8, and 80 mM sodium phosphate. Controls with $Co(NO_3)_2$ were also reported to quench the $Ru(III)(bpy)_3^{3+}$ more slowly than the Co_4POM solution, although no details for these experiments were given. The authors claim[85] that this evidence shows the starting Co_4POM *cannot* be the true WOC and instead favor a POM fragment or decomposition product as a likely WOC when $Ru(III)(bpy)_3^{3+}$ is used as an oxidant. Although this flash photolysis study highlights some potential complexities of working with Co_4POM, a follow-up study by Hill and co-workers[67] shows that under the conditions used for flash photolysis, no measurable O_2 is generated. The lesson here is that the proper interpretation of kinetic data requires the reaction stoichiometry be known—and, ideally, the O_2 evolution kinetics also measured, but this can be problematic to nearly impossible on fast (μs) time scales.

Following the initial work of Hill and co-workers, Stracke and Finke began studies attempting to incorporate the Co_4POM into a hybrid semiconductor-catalyst device for light-driven water oxidation.[148] However, those initial studies of Co_4POM, quickly led, instead, to an electrochemical investigation of whether the Co_4POM is a homogeneous WOC or whether it is a precursor for a heterogeneous CoO_x material.[66] In this investigation, it was found that linear sweep voltammetry of a 500 μM Co_4POM solutions shows an anodic wave at ~1.05 V versus Ag/AgCl which increases more than 10-fold in magnitude during three hours of aging in pH 8, sodium phosphate buffer. This increasing current occurs concomitantly with a 4.3 ± 0.6% decrease in the 580 nm absorbance of Co_4POM—two results which by themselves, pretty much demand that the Co_4POM is evolving to a significantly more active, true WOC. Aging of Co_4POM also results in a 58 ± 2 μM increase in the apparent aqueous $[Co^{2+}]$, which was measured by two complementary methods—by comparing the anodic wave current to $Co(NO_3)_2$ controls and also by cathodic stripping voltammetry.[66] Bulk electrolysis of the Co_4POM solution at 1.1 V versus Ag/AgCl (without aging) results in an increasing catalytic current with time and the deposition of a catalytically active film, that proved to be CoO_x. When this film was removed from the Co_4POM solution and placed into a POM-free solution, the film maintains all of its water oxidation activity. The elemental makeup of this film is consistent with other heterogeneous CoO_x catalysts, containing Co, P, Na, and O as determined by XPS. Importantly, no tungsten was observed in the film, as would be expected if the $[Co_4(H_2O)_2(PW_9O_{34})_2]^{10-}$ was present. Lastly, catalytic controls with a 500 μM Co_4POM solution (aged for 3 h) and a 58 μM $Co(NO_3)_2$ solution (i.e., the amount of aqueous cobalt quantitated in the aged Co_4POM solution) showed quantitatively identical water oxidation activity during a 5 min bulk electrolysis at 1.1 V versus Ag/AgCl, within experimental error (Figure 3). Together, these results all indicate that when a glassy carbon electrode is used as the oxidant source in 500 μM Co_4POM solutions, and under the specific conditions cited earlier, the dominant WOC is an in situ formed CoO_x and not the starting polyoxometalate to 101 ± 12%.[66]

The observation that Co_4POM could be a viable precursor for heterogeneous CoO_x prompted Stracke and Finke to investigate the interesting Co_4POM system under conditions which would favor homogeneous Co_4POM catalysis, if it were present. Their next study therefore looked at the Co_4POM at much lower

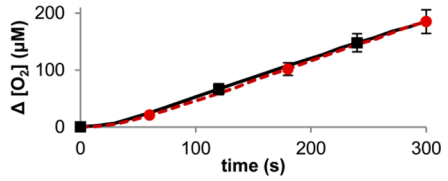

Figure 3. Measured change in dissolved O_2 during bulk electrolysis of either a 500 μM Co_4POM which had been aged for 3 h (red circles) or a 58 μM $Co(NO_3)_2$ control (i.e., the amount of Co^{2+} determined to dissociated from the starting Co_4POM during the 3 h aging) in pH 8, 0.1 M sodium phosphate buffer. Electrolysis was conducted at 1.1 V vs Ag/AgCl at a glassy carbon plate, and O_2 was measured using a fluorescence-based probe from Ocean Optics. Under these conditions, all of the O_2-producing activity (100 ± 12%) in the Co_4POM solution is accounted for by the in situ formed CoO_x catalytic film. The O_2 concentration was recorded every 15 s; the symbols and error bars are given at 60 s intervals for clarity. Reproduced with permission from ref 66.

concentrations and higher electrochemical potentials of 2.5 μM and >1.3 V versus Ag/AgCl, conditions chosen ostensibly to favor water oxidation catalysis by the discrete Co_4POM.[81] Under those new conditions, an irreversible oxidation wave was observed above potentials of 1.25 V versus Ag/AgCl, one which saturated at Co_4POM concentrations of ~5 μM. Comparison to $Co(NO_3)_2$ controls revealed that the anodic wave in Co_4POM solutions occurred at about 200 mV more positive potential than $Co(NO_3)_2$ solutions. Furthermore, the Co_4POM wave shifts by −32 mV/pH unit, whereas the $Co(NO_3)_2$ wave has a −66 mV/pH unit dependence. In addition, the aqueous $[Co^{2+}]$ in 2.5 μM Co_4POM solution was found to be an average 170 nM during a one hour aging experiment. Controls using 200 nM Co^{2+} (added via $Co(NO_3)_2$) demonstrated that this amount of aqueous cobalt(II) now *cannot* account for the water oxidation activity observed in the Co_4POM solution during bulk electrolysis at 1.4 V versus Ag/AgCl (Figure 4). That is, the

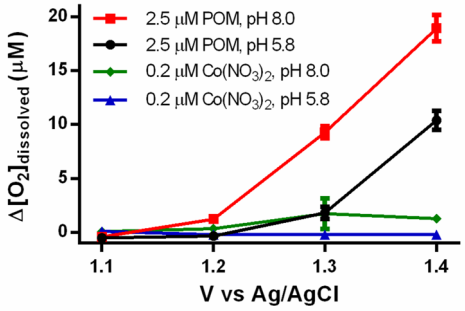

Figure 4. Quantification of O_2 produced during a 60s bulk electrolysis using a glassy carbon electrode at 1.4 V vs Ag/AgCl under the catalyst and pH conditions indicated in the legend (POM = $[Co_4(H_2O)_2(PW_9O_{34})_2]^{10-}$). The controls using 200 nM $Co(NO_3)_2$ were chosen since this is the average $[Co^{2+}]$ in Co_4POM solutions measured over a 1 h aging period in pH 8, 0.1 M sodium phosphate buffer. These data contrast with Figure 3 in that a Co^{2+} to CoO_x WOC is not supported by the data under the different 2.5 μM Co_4POM, 1.4 V oxidation conditions. Reproduced with permission from ref 81.

differing electrochemical features for the Co_4POM and $Co(NO_3)_2$, plus the controls using the independently measured amount of Co^{2+}, provide strong evidence that CoO_x formed *at least solely from* Co^{2+} is not the dominant WOC at these

dx.doi.org/10.1021/cs4011716 | ACS Catal. 2014, 4, 909−933

micromolar concentrations of Co_4POM—a conclusion which highlights the importance reaction conditions can play in determining the true WOC, as others have also stressed.[6,7,67,81]

An additional question, relevant to the electrochemically driven Co_4POM system, is whether the polyoxometalate could transform into a heterogeneous CoO_x catalyst under the oxidative reaction conditions? To answer this question, Stracke and Finke started by measuring the Co_4POM concentration via HPLC both before, and after, bulk electrolysis at 1.4 V versus Ag/AgCl. They found that the Co_4POM concentration decreased by 2.7 ± 7.3 and 9.4 ± 5.1% during a 60 s electrolysis in pH 8.0 and 5.8 sodium phosphate solutions.[81] At pH 8, quantification of the postreaction solution $[Co^{2+}]$ shows an increase of 50 ± 34 nM relative to the prereaction solution. Meanwhile, controls with predeposited CoO_x catalysts revealed that if only 3.4 or 8.3% of the Co_4POM were converted into a CoO_x catalyst, then that would account for all of the observed catalytic activity at pH 8.0 and 5.8. That is, the observed instability of the Co_4POM at 1.4 V versus Ag/AgCl and the high activity of the CoO_x controls do not yet allow one to distinguish between an authentic Co_4POM and a heterogeneous CoO_x catalyst under the reaction conditions of that study designed to favor Co_4POM-based, electrochemically driven water oxidation catalysis.

In a 2013 study by Hill and co-workers, additional evidence is provided which is consistent with the Co_4POM being an active WOC when using chemical and photochemical oxidation by $Ru(III)(bpy)_3^{3+}$.[67] First, the stability of Co_4POM was measured under noncatalytic conditions of 2 μM Co_4POM, pH 8, and 80 mM sodium borate, where 70 nM Co^{2+} dissociated from the parent POM over 3 h. Measurement of the $Ru(bpy)_3^{3+}$ loss kinetics using either 2 μM Co_4POM or 2 μM Co_4POM plus 0.1 μM $Co(NO_3)_2$ in the presence of ∼1 mM $Ru(bpy)_3^{3+}$ resulted in oxidant-loss rates which were within 5% of one another. Other kinetic controls with 0.5 μM $Co(NO_3)_2$ showed sigmoidal $Ru(bpy)_3^{3+}$ reduction kinetics and reduction rates which were comparable, or slower, than 2 μM Co_4POM. Although these results are consistent with a POM catalyst, one cannot rigorously compare $Ru(bpy)_3^{3+}$ reduction rates with O_2 evolution activity since a significant portion of the reduction rate corresponds to unproductive bpy ligand oxidation reactions.

More direct evidence for a Co_4POM catalyst was provided by Hill and co-workers in photochemical experiments where controls using 0.15 μM $Co(NO_3)_2$ produced O_2 in the same (negligible) amount as controls with no catalyst.[67] Photochemical experiments with 2 μM Co_4POM under the same conditions resulted in 24.2 ± 0.1% O_2 yields. However, multiple other photochemical controls with $Co(NO_3)_2$ showed O_2 yields which were comparable or greater than Co_4POM experiments when equivalent amounts were used; for example, when 2 μM $Co(NO_3)_2$ was used, 40.8 ± 0.5% O_2 yields were seen. That is, the Co_4POM stability under the reaction conditions must still be quantified to rule out the possibility of an in situ formed CoO_x material contributing to the activity.

Another line of evidence for Co_4POM catalysis provided by the Hill et al. involves a series of extraction experiments and controls.[67] First, a standard 2 μM Co_4POM photochemical reaction was run which produced the expected amount of O_2. Following the reaction, the POM was extracted using a toluene/tetra-*n*-heptylammonium nitrate ($THpANO_3$) procedure. When fresh $Ru(bpy)_3^{2+}$ and $S_2O_8^{2-}$ were added to the solution, a subsequent photochemical reaction produced no O_2. To ensure that the residual toluene and $THpANO_3$ do not influence the reaction, a control was conducted where an aqueous solution of the sodium borate buffer was subjected to the extraction procedure, followed by addition of 2 μM Co_4POM, $Ru(bpy)_3^{2+}$ and $S_2O_8^{2-}$; when this solution was illuminated, it produced the same amount of O_2 as a standard (unextracted) reaction. A photochemical control using a 2 μM $Co(NO_3)_2$ solution which had undergone extraction showed that this method does not interfere with Co^{2+} catalyst precursors. The authors also claim that the extraction procedure does not interfere with a CoO_x catalyst. Overall, the precatalytic Co_4POM stability measurement, controls with the measured amount of dissociated Co^{2+}, and extraction experiments are all consistent with a homogeneous POM catalyst.

Most recently, Stracke and Finke have conducted a kinetic and mechanistic analysis of this same Co_4POM plus $Ru(bpy)_3^{3+}$ water oxidation system.[117] Under initial conditions of 0.5−2.0 μM Co_4POM, 500−1500 μM $Ru(bpy)_3^{3+}$, 50−200 μM $Ru(bpy)_3^{2+}$, pH 6.8−7.8, and 0.3 M sodium phosphate, they measured both the O_2 evolution kinetics and $Ru(bpy)_3^{3+}$ reduction kinetics en route to determining the empirical rate law in eq 1:

$$\frac{-\mathrm{d}[\mathrm{Ru(III)(bpy)_3^{3+}}]}{\mathrm{dt}} = (k_1 + k_2)\frac{[\mathrm{Ru(III)(bpy)_3^{3+}}][\mathrm{Co_4POM}]_{\mathrm{soluble}}}{[\mathrm{H^+}]} \quad (1)$$

Parameters k_1 and k_2 correspond to the observed rate constants for the parallel O_2 evolution and bpy ligand oxidation reactions, and $[Co_4POM]_{soluble}$ is the amount of soluble POM. In comparison, Co^{2+} controls showed a first-order dependence of the O_2 evolution rate on $[Co^{2+}]$, but a zero-order dependence of the O_2 evolution rate on $[Ru(bpy)_3^{3+}]$. That is, the O_2 evolution rate law is different for the Co_4POM and Co^{2+} precatalysts. Overall, this kinetic contrast argues strongly that the true catalyst is different in these two systems, although the precise identity and atomic composition of the true catalyst remains unknown.

In other cobalt POM studies, Song et al. looked at a variety of cobalt substituted Keggin type POMs (Figure 5) and found

Figure 5. General structural model for $[XYW_{11}O_{39}]^{n-}$ where blue polyhedral are WO_6, red = O, and white = H. For $Co(III)Co(II)W_{11}O_{39}^{7-}$, orange = CoO_4, purple = Co. For ruthenium analogues $[Ru(H_2O)SiW_{11}O_{39}]^{5-}$, $[Ru(H_2O)GeW_{11}O_{39}]^{5-}$, and $[Ru(H_2O)PW_{11}O_{39}]^{4-}$, purple = Ru, and orange = SiO_4, GeO_4, and PO_4.

the $Co(III)Co(II)W_{11}O_{39}^{7-}$ showed a water oxidation TOF of 0.5 s^{-1} (for an unknown rate law) and a 30% O_2 yield when using photochemically generated $Ru(III)(bpy)_3^{3+}$.[68] These authors provided evidence that the active catalyst is homogeneous, including the absence of any at least detectable particles by dynamic light scattering after 10 min of illumination. However, and curiously, when only 0.1 mol % of Co^{2+} was added to the $Co(III)Co(II)W_{11}O_{39}^{7-}$ reaction solution (where $[Co^{2+}]$ +

dx.doi.org/10.1021/cs4011716 | ACS Catal. 2014, 4, 909−933

$[Co(III)Co(II)W_{11}O_{39}^{7-}]$ = 15 μM), particles were observable *both before and after photolysis*—that is, it is not clear why such a small amount of Co^{2+} plus the $Co(III)Co(II)W_{11}O_{39}^{7-}$ forms particles prior to irradiation, but 1 mM $Ru(II)(bpy)_3^{2+}$ plus the polyoxometalate does not. Also, a control with 45 nM $Co(NO_3)_2$ showed no observable water oxidation activity. UV–vis spectroscopy and flash photolysis of aged $Co(III)Co(II)W_{11}O_{39}^{7-}$ solutions further attest to the hydrolytic stability of this POM. Cyclic voltammetry of the $Co(III)Co(II)W_{11}O_{39}^{7-}$ in comparison with $Co(NO_3)_2$ controls is also consistent with Co^{2+} not being present in the solution before the photolysis reaction. Interestingly, the $Co(II)Co(II)W_{11}O_{39}^{8-}$ oxidation state of the POM is not hydrolytically stable in solution, but instead, it forms bulk $Co(OH)_2$ over a 1 h aging experiment in the pH 9 sodium borate buffer. This result is intriguing, because it is possible, if not likely, that the $Co(III)Co(II)W_{11}O_{39}^{7-}$ goes through this lower oxidation state during water oxidation catalysis.

Experiments consistent with $Co(III)Co(II)W_{11}O_{39}^{7-}$ stability under reaction conditions include precipitation of the POM from postphotolysis solutions with subsequent characterization by EDX and IR (Figure 6).[68] Also, after precipitation and

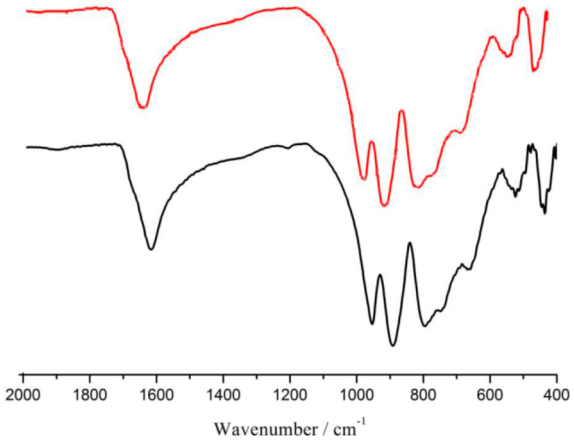

Figure 6. Comparison of fresh $Co(III)Co(II)W_{11}O_{39}^{7-}$ (top) and the material isolated from a postphotocatalytic reaction (bottom) via acetone addition and centrifugation. The similarity between the spectra indicates the starting POM remains qualitatively intact during the reaction. Additional controls using authentic CoO_x are needed to help determine if CoO_x can be observed via this isolation/characterization method. Reproduced with permission from ref 68.

centrifugation, no residual particles were observed in the reaction solution by DLS. Redissolution of the precipitated POM also showed no observable particles by DLS and subsequent photocatalytic testing showed similar, ~10% lower, activity for the redissolved $Co(III)Co(II)W_{11}O_{39}^{7-}$ compared to the initial $Co(III)Co(II)W_{11}O_{39}^{7-}$ solution. As noted previously, although these types of phenomenological tests are consistent with the starting material being a WOC, quantitative knowledge of the speciation *during* the reaction is needed to unequivocally identify the active catalyst. Hence, the true catalyst in the case of the $Co(III)Co(II)W_{11}O_{39}^{7-}$ precatalyst remains uncertain.

Another interesting cobalt polyoxometalate system is $\{Co_9(H_2O)_6(OH)_3(HPO_4)_2(PW_9O_{34})_3\}^{16-}$ (Co_9POM, which is shown in Figure 7) since it is a trimeric analogue of the Co_4POM dimer. In a study by Galán-Mascarós and co-workers,

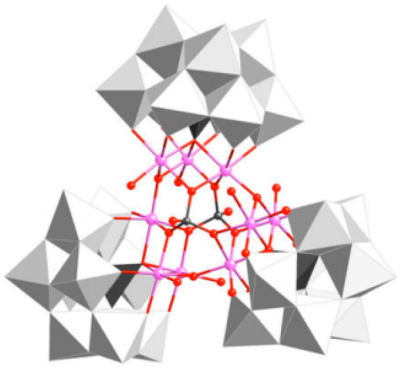

Figure 7. Mixed polyhedral/ball-and-stick model of $\{Co_9(H_2O)_6(OH)_3(HPO_4)_2(PW_9O_{34})_3\}^{16-}$ where white polyhedral = WO_6, black = PO_4 or P, pink = Co, and red = O. Hydrogen atoms are not shown for clarity. Reproduced with permission from ref 79.

bulk electrolysis of the Co_9POM at 1.41 V versus NHE resulted in the formation of a catalytic film on the electrode in pH 7 sodium phosphate buffer.[79] This film, which contains cobalt and phosphorus by EDX, maintains its activity when it is transferred to a POM-free solution—similar to other in situ formed, heterogeneous CoO_x catalysts. In order to help distinguish whether any of the activity was due to authentic Co_9POM water oxidation catalysis, 2,2′-bipyridine was added to the electrolysis solution which resulted in a 40-fold decrease in the oxidation current at 1.41 V versus NHE; no CoO_x film was observed post the 2,2′-bipyridine addition on the postelectrolysis FTO electrode by SEM or EDX. Concurrent with electrolysis, a $[Co(III)(bpy)_3]_4K_{4-x}Na_x[Co_9POM]$ precipitates from the solution, and the dissolved $[Co_9POM]$ decreases by 30%, as determined by UV–vis spectroscopy. Cyclic voltammetry was also used to characterize Co_9POM, which shows a peak at 0.75 V and a catalytic wave at 1.10 V; when 2,2′-bipyridine is added, only a 1.10 V catalytic wave onset is seen—evidence which the authors claim rules out CoO_x when bpy is present. However, due to the observed instability of the Co_9POM under oxidizing conditions and the similar onset potential for the catalytic current, it is also possible that the Co_9POM is simply being converted into a transiently stable CoO_x catalyst. Controls with authentic CoO_x are needed to rule out, or support, this possibility.

Stronger evidence for homogeneous catalysis was found for Co_9POM when NaClO was used as an oxidant at pH 8.[79] For these NaClO oxidation experiments, no change in the UV–vis spectrum of the Co_9POM was observed, dynamic light scattering showed the same size particles of ~1 nm before and after the experiment (i.e., the approximate size of the Co_9POM), and addition of bipyridine does not significantly change the O_2 yields or kinetics. The POM can also be recovered from the solution by addition of excess alkali cation and was the same as the initial, unreacted Co_9POM sample (as judged by IR and XRD). The only possible evidence that Co_9POM transforms into a more active WOC during the reaction is the slightly sigmoidal shape of the O_2 versus time plot when the pH is 7 or at 15 °C ($[Co_9POM]$ = 1.0 mM, $[NaClO]$ = 100 mM). Alternatively, and as noted in the introduction, a sigmoidal O_2 evolution plot could be due to the slow O_2 solution-to-gas mass transfer. This remaining question could be resolved by measuring the O_2 generation rate in solution with a faster sensor or by increasing the stirring rate to accelerate the O_2 solution/gas equilibration.

dx.doi.org/10.1021/cs4011716 | *ACS Catal.* 2014, 4, 909–933

A subsequent study by Galán-Mascarós and co-workers investigated Co_9POM (specifically $Cs_{15}K\{Co_9(H_2O)_6(OH)_3(HPO_4)_2(PW_9O_{34})_3\}$) when supported in a carbon paste electrode. When the electrode potential is held at 1.3 V versus NHE in pH 7 sodium phosphate buffer, the oxidation current decreases slightly over the first ∼30 min and then maintains its activity over greater than 8 h. Controls consistent with POM catalysis showed that even 125 μmol of Co_3O_4 were ∼2−3 times less active than just 2 μmol of Co_9POM, although the authors acknowledge that catalytic surface areas were not taken into account in this comparison. Additionally, the IR, EDX, and XRD characterization of the Co_9POM−carbon electrode appear qualitatively the same before and after an 8 h electrolysis. However, since these characterization techniques measure the bulk of the electrode material, more surface-sensitive techniques such as XPS could assist in determining whether the true electrocatalyst is the Co_9POM or is a surface CoO_x material.

In 2012, Car et al. studied photochemical water oxidation with $[Co_4(H_2O)_2(SiW_9O_{34})_2]^{12-}$, which is the silicon(IV) core analogue of $[Co_4(H_2O)_2(PW_9O_{34})_2]^{10-}$ (Figure 2).[69] Initial UV−vis stability measurements indicate that up to 25% of the POM decomposes during a 2.5 h period in pH 5.8 $NaSiF_6$ buffer. Despite this decomposition, the authors claim that the catalytic activity resides in a precipitated $[Co_4(H_2O)_2(SiW_9O_{34})_2]^{12-}$:$[Ru(bpy)_3^{2+}]$ material which forms immediately upon combining the cobalt POM and the photosensitizer. FTIR of the pre- and postcatalytic precipitate indicate the presence of $[Co_4(H_2O)_2(SiW_9O_{34})_2]^{12-}$; this precipitate can also be reused with moderate, ∼50% loss in O_2 evolution activity. Preliminary controls with Co^{2+} were also reported. Additional speciation data and characterization of the precipitate's surface may provide further evidence for the true WOC.

Zhu et al. used $[Co_4(\mu\text{-}OH)(H_2O)_3(Si_2W_{19}O_{70})]^{11-}$ under typical $Ru(bpy)_3^{2+}$ plus $S_2O_8^{2-}$ photochemical conditions to generate O_2 from water, as shown in Figure 8.[70,71] This POM starting material was found to be even less stable than other tetra-cobalt POMs, such as $[Co_4(H_2O)_2(PW_9O_{34})_2]^{10-}$, under noncatalytic conditions. UV−vis spectroscopy showed the $[Co_4(\mu\text{-}OH)(H_2O)_3(Si_2W_{19}O_{70})]^{11-}$ transforming into other species over a period of hours to days. From these aged solutions, Zhu recovered $K_{10}Na[\{Co(H_2O)\}(\mu\text{-}H_2O)_2K\{Co(H_2O)_4\}(Si_2W_{18}O_{66})]$ and $[Co(H_2O)SiW_{11}O_{39}]^{6-}$. Stoichiometric analysis and UV−vis data indicate that aqueous Co^{2+} is also released during this process. To probe whether the decomposition products are contributing to catalysis, controls were completed with both $K_{10}Na[\{Co(H_2O)\}(\mu\text{-}H_2O)_2K\{Co(H_2O)_4\}(Si_2W_{18}O_{66})]$ and $[Co(H_2O)SiW_{11}O_{39}]^{6-}$ under photochemical conditions where three times less activity, and no O_2 evolution activity, were observed, respectively. Aging the $[Co_4(\mu\text{-}OH)(H_2O)_3(Si_2W_{19}O_{70})]^{11-}$ solution for 3−4 weeks followed by catalytic testing results in 20−30% lower O_2 yields compared to the fresh POM precursor. Although the authors claim that $[Co_4(\mu\text{-}OH)(H_2O)_3(Si_2W_{19}O_{70})]^{11-}$ could be the active WOC, they acknowledge the possibility that dissociated aqueous Co^{2+} (i.e., in situ formed CoO_x) contributes to catalysis. Until the catalytic contribution of heterogeneous CoO_x is known, the claim of a homogeneous POM catalyst remains uncertain for this case as well.

Another set of Keggin dimers with dicobalt, dibismuth bridges were studied by Guo et al.[86] When 5.6 μM $Na_9H_5[Co_2Bi_2(\alpha\text{-B-}CoW_9O_{34})_2]$ or $Na_9H_5[Co_2Bi_2(\beta\text{-B-}CoW_9O_{34})_2]$ were illuminated with a 300 W xenon lamp in the presence of 1.0 mM $Ru(bpy)_3^{2+}$ and 5.0 mM $S_2O_8^{2-}$ in pH 7.4 sodium phosphate buffer, up to 18 μmol of O_2 (TON = ∼32) was produced. Stability of these POMs under noncatalytic conditions was examined by measuring the cyclic voltammetry response over a 3 h aging period. Because no change in the CV was observed, the authors conclude that the POMs are stable. Unfortunately, no other data speaks to the speciation or stability of the POMs under the reaction conditions. Hence, the true catalyst is unknown in this case.

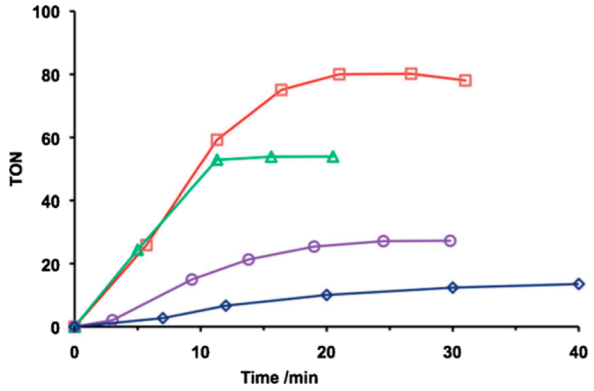

Figure 8. Calculated turnover number (TON = mols O_2 generated per mol $[Co_4(\mu\text{-}OH)(H_2O)_3(Si_2W_{19}O_{70})]^{11-}$) for a photocatalytic reaction containing 1.0 mM $Ru(bpy)_3^{2+}$, 5 mM $S_2O_8^{2-}$, 25 mM buffer, and 10 μM $[Co_4(\mu\text{-}OH)(H_2O)_3(Si_2W_{19}O_{70})]^{11-}$. The buffers used are pH 9 sodium borate (red squares), pH 8 sodium borate (green triangles), pH 8 equi-molar sodium phosphate/sodium borate (purple circles), and pH 7.2 sodium phosphate (blue diamonds). Note the slightly sigmoidal kinetics seen in the bottom two curves; additional in operando speciation and O_2 experiments are therefore needed to determine whether the induction period is due to slow solution-to-gas transfer of the O_2 (as suggested by the authors) or whether the POM is evolving into a faster WOC. Alternatively, one could simply measure the solution concentration of O_2 to determine whether the induction period is real or an artifact. Reproduced with permission from ref 70.

Others have observed instability of cobalt POMs under electrocatalytic conditions. Lai et al. drop cast cobalt-polyoxotitanates, $[Ti_{12}O_{15}(O^iPr)_{17}]^+[(CoBr)_6Ti_{15}O_{24}(O^iPr)_{18}(Br)]^-$ and $[(CoI)Ti_{11}O_{14}(O^iPr)_{17}]$, onto FTO electrodes and then biased the electrodes at 1.35 V versus NHE where catalytic oxidation was observed.[110] Before electrolysis, SEM/EDX of the drop cast film shows islands which contain cobalt but no phosphorus. In contrast, the postcatalysis electrode shows islands with a Co:P of 1:9 plus a new film between the islands which has a Co/P of 2:1—evidence that POMs can transform into heterogeneous CoO_x WOCs under oxidizing conditions. Although a CoO_x material likely contributes to the overall electrocatalytic activity of the system, following the decomposition of the $[Ti_{12}O_{15}(O^iPr)_{17}]^+[(CoBr)_6Ti_{15}O_{24}(O^iPr)_{18}(Br)]^-$ and $[(CoI)Ti_{11}O_{14}(O^iPr)_{17}]$ POMs over time and determining whether this corresponds to increasing or decreasing activity may help distinguish whether the starting POM might also be contributing to the activity.

A final cobalt-based example of electrocatalytic water oxidation uses a carbon-paste-supported $[Hpy]_2\{[Co(4,4'\text{-}Hbpy)_2(H_2O)_2][SiCoW_{11}O_{39}]\}$.[149] The starting POM was characterized by X-ray crystallography, IR spectroscopy, and elemental analysis. Although the authors claim catalytic water oxidation by the POM, the only evidence provided is cyclic voltammetry showing an irreversible oxidation wave at ∼1300 mV versus Ag/AgCl.

dx.doi.org/10.1021/cs4011716 | ACS Catal. 2014, 4, 909−933

In summary of this section on cobalt POMs, when beginning with cobalt POMs, a wide variety of characterization techniques have been used to examine these materials for their *qualitative* stability under water oxidation reaction conditions. However, there is a lack of *quantitative stability measurements*, with the exception of electrochemical studies of Co_4POM and Co_9POM.[81,79] It seems possible that this dearth of information may be a result of using $Ru(bpy)_3^{3+}$ as an oxidant and the resulting complications of POM^{n-}:$Ru(bpy)_3^{3+/2+}$ formation and precipitation, or the need to work at low micromolar concentrations to minimize such precipitates. Study of cobalt POMs and determination of the true catalysts therein would therefore benefit greatly from the development of either a neutral or anionic terminal oxidant, or continued use of electrochemical oxidation methods.

3.2. Ruthenium. *3.2.1. Non-POM Ruthenium Precatalysts.* Ruthenium has been reported as a homogeneous WOC active site more than any other metal.[12,15−17] Despite the widespread use of ruthenium in homogeneous WOC precursors, we have found only one literature example which provides substantial evidence that a homogeneous ruthenium complex (ruthenium red, $[(NH_3)_5RuORu(NH_3)_4ORu(NH_3)_5]^{6+}$) irreversibly decomposes into a possibly polymeric ruthenium material upon oxidation by cerium(IV) ammonium nitrate (Ce(IV)).[150] This study relies primarily on UV−vis spectroscopy to characterize the transformation and to demonstrate that decomposition occurs prior to chemically driven water oxidation catalysis. Studies by Collin and Sauvage also observe the formation of brown and/or black precipitates when starting with Ce(IV) and a variety of ruthenium precursors including $RuCl_3$, $Ru(bpy)_2(CO_3)$, or $[(bpy)_2(H_2O)RuORu(OH_2)(bpy)_2]^{4+}$; these authors therefore conclude that bulk RuO_2 (or other decomposition products) may be contributing to the observed catalysis in these cases.[151] Liu et al. suggest in their WOC review that the difficultly in identifying a heterogeneous RuO_2 catalyst might have to do with the nondescript visible absorption spectrum associated with ruthenium oxide. Alternatively, the relative strength of ruthenium metal−ligand bonds may account for the observed robustness under water oxidation conditions. Regardless of whether homogeneous ruthenium WOC stability is real or perceived, more thorough study of ruthenium-based precatalysts in water oxidation catalysis should continue.

3.2.2. Ruthenium POM Precatalysts. In 2008, Hill and co-workers[73] and Sartorel and co-workers[72] independently reported catalytic water oxidation using a tetra-ruthenium POM, $[Ru_4(\mu\text{-}O)_4(\mu\text{-}OH)_2(H_2O)_4(\gamma\text{-}SiW_{10}O_{36})_2]^{10-}$ shown in Figure 9, in conjunction with either a $Ru(bpy)_3^{3+}$ oxidant (pH 7.2) or a Ce(IV) oxidant (pH 0.6). Evidence for POM stability was collected by characterizing the different oxidation/protonation states of the ruthenium POM.[64,74] These complexes were generated either electrochemically via bulk electrolysis or by addition of 1−4 equivalents of oxidant. Characterization was accomplished by electrochemical methods,[82] EPR, resonance Raman, and EXAFS/XANES.[104] The $[Ru_4(\mu\text{-}O)_4(\mu\text{-}OH)_2(H_2O)_4(\gamma\text{-}SiW_{10}O_{36})_2]^{10-}$ could also be recovered from a reaction solution after 8 equivalents of Ce(IV) were added followed by a 1 h aging time and precipitation of the POM as the Cs^+ salt.[72] FTIR and resonance Raman of the precipitate appear qualitatively the same as the prereaction $[Ru_4(\mu\text{-}O)_4(\mu\text{-}OH)_2(H_2O)_4(\gamma\text{-}SiW_{10}O_{36})_2]^{10-}$—evidence that at least some of the POM remains intact.[72] However, UV−vis spectroscopy indicates slow decomposition of the starting POM below pH 1.[72] When

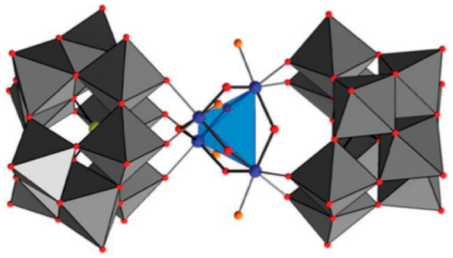

Figure 9. Mixed polyhedral/ball-and-stick structure of $[Ru_4(\mu\text{-}O)_4(\mu\text{-}OH)_2(H_2O)_4(\gamma\text{-}SiW_{10}O_{36})_2]^{10-}$ where gray polyhedra = WO_6, blue = Ru, red = O(H), orange = OH_2. Reproduced with permission from ref 73.

7000 to 2.4×10^5 equivalents of Ce(IV) were used, O_2 evolution kinetics are first-order in $[Ru_4(\mu\text{-}O)_4(\mu\text{-}OH)_2(H_2O)_4(\gamma\text{-}SiW_{10}O_{36})_2]^{10-}$ (initial [POM] = 4.5−145 μM).[72] Additional evidence in support of a homogeneous POM WOC includes controls using $K_4Ru_2OCl_{10}$ (i.e., the ruthenium precursor used in the $[Ru_4(\mu\text{-}O)_4(\mu\text{-}OH)_2(H_2O)_4(\gamma\text{-}SiW_{10}O_{36})_2]^{10-}$ synthesis), which show a significant induction period and an approximately 10-fold slower O_2 evolution rate compared to $[Ru_4(\mu\text{-}O)_4(\mu\text{-}OH)_2(H_2O)_4(\gamma\text{-}SiW_{10}O_{36})_2]^{10-}$.[72]

Complementary tests and controls done by Hill and co-workers using $RuCl_3$ in the presence and absence of the $[\gamma\text{-}SiW_{10}O_{36}]^{8-}$ POM building block reveal $Ru(bpy)_3^{3+}$ reduction rates 100 times slower starting with $RuCl_3$ than with $[Ru_4(\mu\text{-}O)_4(\mu\text{-}OH)_2(H_2O)_4(\gamma\text{-}SiW_{10}O_{36})_2]^{10-}$ and which produce <11% O_2 yields.[73] Kinetic experiments, using 1−8 μM $[Ru_4(\mu\text{-}O)_4(\mu\text{-}OH)_2(H_2O)_4(\gamma\text{-}SiW_{10}O_{36})_2]^{10-}$ plus 0.6−2.3 mM $Ru(bpy)_3^{3+}$ at pH 7.2, resulted in an empirical rate law which is first-order in POM and first-order in the $Ru(bpy)_3^{3+}/Ru(bpy)_3^{2+}$ ratio.[74] Additionally, consistent with the absence of observable heterogeneous catalyst, no particles were detected by DLS or SAXS techniques in the post reaction $[Ru_4(\mu\text{-}O)_4(\mu\text{-}OH)_2(H_2O)_4(\gamma\text{-}SiW_{10}O_{36})_2]^{10-}$ solutions, although particle detection limits for these methods were not reported.

Subsequently, other studies of the $[Ru_4(\mu\text{-}O)_4(\mu\text{-}OH)_2(H_2O)_4(\gamma\text{-}SiW_{10}O_{36})_2]^{10-}$ complex have investigated incorporation into photochemically driven systems including the common $h\nu$ + photosensitizer + $S_2O_8^{2-}$ setup where the photosensitizer can be $Ru(bpy)_3^{2+}$ or related derivatives such as $[Ru(II)\{(\mu\text{-dpp})Ru(II)(bpy)_2\}_3]^{8+}$ (dpp =2,3-bis(2′-pyridyl)pyrazine).[118−120] Studies using the 1.0 mM $Ru(bpy)_3^{2+}$ photosensitizer formed a precipitate with the starting POM when $[Ru_4(\mu\text{-}O)_4(\mu\text{-}OH)_2(H_2O)_4(\gamma\text{-}SiW_{10}O_{36})_2]^{10-}$ concentrations were above 5 μM;[119] concomitant with this precipitation, O_2 evolution rates did not increase when the POM concentration was above 2.5 μM. That is, O_2 evolution kinetics appear to scale with the amount of soluble ruthenium polyoxometalate. Importantly, and consistent with the $Ru(bpy)_3^{3+}$ and Ce(IV) oxidant studies, photochemical $RuCl_3$ controls showed no O_2, and RuO_2 controls resulted in O_2 evolution rates which were 10−20 times slower than when starting with the $[Ru_4(\mu\text{-}O)_4(\mu\text{-}OH)_2(H_2O)_4(\gamma\text{-}SiW_{10}O_{36})_2]^{10-}$ complex.[119] Although these observations are *consistent* with a POM catalyst, the RuO_2 controls should, if possible, be corrected for the number of active sites so that a more direct comparison of the per-site activity can be made. Overall, however, the multiple studies, extensive characterization of $[Ru_4(\mu\text{-}O)_4(\mu\text{-}OH)_2(H_2O)_4(\gamma\text{-}SiW_{10}O_{36})_2]^{10-}$, and multiple kinetic controls suggests that this complex is a homogeneous WOC when using chemically and photochemically driven oxidation.

dx.doi.org/10.1021/cs4011716 | *ACS Catal.* 2014, 4, 909−933

The tetra-ruthenium POM $[Ru_4(\mu\text{-}O)_4(\mu\text{-}OH)_2(H_2O)_4(\gamma\text{-}SiW_{10}O_{36})_2]^{10-}$ has also been studied using electrochemically driven oxidation. Toma et al. prepared and tested $[Ru_4(\mu\text{-}O)_4(\mu\text{-}OH)_2(H_2O)_4(\gamma\text{-}SiW_{10}O_{36})_2]^{10-}$ which had been loaded onto polyamidoamine-functionalized multiwalled carbon nanotubes.[83] These functionalized electrodes can be cycled at least nine times up to 1.6 V versus Ag/AgCl without significant changes in the observed oxidation current. Although impressive *pre*catalysis characterization of the electrode via HRTEM, STEM, EDX, SAXS, and Raman spectroscopy indicate the presence of the intact POM, no *post*catalysis characterization was reported. Without knowledge of the $[Ru_4(\mu\text{-}O)_4(\mu\text{-}OH)_2(H_2O)_4(\gamma\text{-}SiW_{10}O_{36})_2]^{10-}$ stability under the reaction conditions and without catalytic controls (e.g., RuO_2), it is difficult to make any firm conclusions about the active catalyst in this interesting, but complex, electrochemical water oxidation system.

Another tetra-ruthenium POM, $[(\gamma\text{-}PW_{10}O_{36})_2Ru_4O_5(OH)(H_2O)_4]^{9-}$ which incorporates a phosphotungate backbone, was also reported as a photochemically driven WOC.[75] Observation of two reversible protonation equilibria and seven reversible cyclic voltammetry waves indicate the initial stability of the POM in solution. Also, consistent with the $[Ru_4(\mu\text{-}O)_4(\mu\text{-}OH)_2(H_2O)_4(\gamma\text{-}SiW_{10}O_{36})_2]^{10-}$ analogue studies, the O_2 evolution rate depends only weakly on the initial $[(\gamma\text{-}PW_{10}O_{36})_2Ru_4O_5(OH)(H_2O)_4]^{9-}$ concentration. That is, the primary evidence $[(\gamma\text{-}PW_{10}O_{36})_2Ru_4O_5(OH)(H_2O)_4]^{9-}$ might be homogeneous is that it behaves similar to $[Ru_4(\mu\text{-}O)_4(\mu\text{-}OH)_2(H_2O)_4(\gamma\text{-}SiW_{10}O_{36})_2]^{10-}$, where evidence for homogeneous catalysis is stronger. Further kinetic and other studies addressing the true catalyst when beginning with $[(\gamma\text{-}PW_{10}O_{36})_2Ru_4O_5(OH)(H_2O)_4]^{9-}$ would be welcome, however.

An interesting triruthenium substituted Keggin silicotungstate, $[\{Ru_3O_3(H_2O)Cl_2\}(SiW_9O_{34})]^{7-}$, was used as a starting material in a 1.0 mM $Ru(bpy)_3^{2+}$ plus 5.0 mM $S_2O_8^{2-}$ photochemically driven system (Figure 10).[69] Contrary to most other POM WOC studies, Car et al. hypothesize that precipitated ($[\{Ru_3O_3(H_2O)Cl_2\}(SiW_9O_{34})]^{7-}$):$[Ru(bpy)_3^{2+}]$ is the active catalytic species. Consistent with this assertion, a precipitate forms upon combining the triruthenium POM and the $Ru(bpy)_3^{2+}$ photosensitizer. This precipitate contains IR bands characteristic of the intact POM at approximately 976, 948, and 873 cm^{-1} in both the initial POM and also after a catalytic run with isolation by centrifugation. The supernatant of the centrifuged postcatalysis solution contains no residual activity even when fresh $Ru(bpy)_3^{2+}$ and $S_2O_8^{2-}$ were added—evidence that the true catalyst resides primarily in the solid state.

Stability of the starting $[\{Ru_3O_3(H_2O)Cl_2\}(SiW_9O_{34})]^{7-}$ under noncatalytic conditions was investigated by UV–vis where a 3.5% decrease in the 440 nm absorbance over 3 h is observed; no additional decomposition is seen for the POM in the presence of $S_2O_8^{2-}$ and illumination over 2.5 h.[69] Photochemical controls with $RuCl_3$ under otherwise standard conditions did not result in O_2 formation. Further evidence of the true catalyst could include determining the fate of the 3.5% unstable fraction of the POM and looking into whether that form of ruthenium possesses any catalytic activity. XPS of the pre- and postcatalysis ($[\{Ru_3O_3(H_2O)Cl_2\}(SiW_9O_{34})]^{7-}$):$[Ru(bpy)_3^{2+}]$ solid could also potentially help determine whether the surface of the material changes during catalysis or not.

In a different ruthenium POM dimer, Howells et al. claimed electrocatalytic water oxidation when starting with what is believed to be[152] $[Ru(III)_2Zn_2(H_2O)_2(ZnW_9O_{34})_2]^{14-}$ and

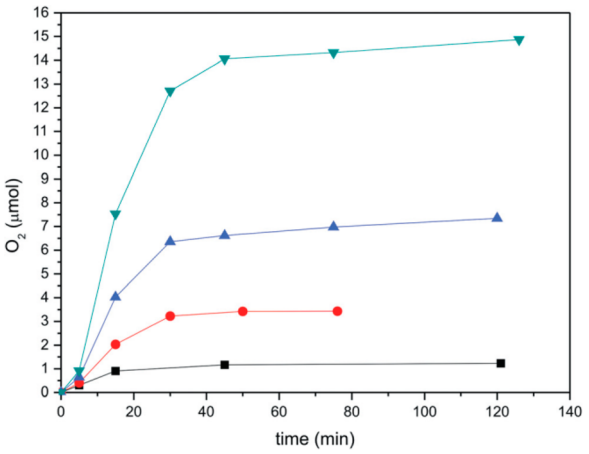

Figure 10. O_2 evolution kinetics for $[\{Ru_3O_3(H_2O)Cl_2\}(SiW_9O_{34})]^{-}$ in the presence of 1 mM $Ru(bpy)_3^{2+}$, 5 mM $S_2O_8^{2-}$, 20 mM Na_2SiF_6 buffer (pH 5.8), and 465 nm illumination. [POM] = 16 μM (black squares), 21 μM (red circles), 31 μM (blue triangles), and 50 μM (green inverted triangles). O_2 was measured by GC of the reaction headspace. The sigmoidal shape of these kinetic curves indicate the need for experiments aimed at identifying whether the shape is determined by solution-to-gas transfer limitations or by changes in the active catalyst, as discussed in section 2.4. Reproduced with permission from ref 69.

using a gold electrode in pH 8 phosphate buffer.[123] Oxygen evolution was observed to be potential dependent for the $[Ru(III)_2Zn_2(H_2O)_2(ZnW_9O_{34})_2]^{14-}$, whereas controls using a di-Zn POM (whose structure was not specified) or $[Ru(H_2O)PW_{11}O_{39}]^{4-}$ showed no O_2 evolution activity up to 1.05 V versus NHE. The current–overpotential (Tafel) relationship was also measured to be 120 mV/decade for $[Ru(III)_2Zn_2(H_2O)_2(ZnW_9O_{34})_2]^{14-}$; heterogeneous RuO_2 and perovskite materials typically exhibit slopes of 60 or 120 mV/decade. That is, a pure RuO_2 WOC is most likely *not* present in this POM system, but the possibility of a catalytic contribution from a different, unknown heterogeneous material has not been ruled out.

If the active catalyst is indeed the starting $[Ru(III)_2Zn_2(H_2O)_2(ZnW_9O_{34})_2]^{14-}$, then it is not clear what the active site might be since the ruthenium atoms are on the *interior* of the complex and are not coordinated to terminal aquo, hydroxo, or oxo ligands. This problem is further complicated by the observation that only ~1.24 equivalents of ruthenium are incorporated into the two central positions according to XRD refinement, whereas the other 0.76 equivalents correspond to tungsten; the XRD calculation also contrasts with the elemental analysis which indicates the presence of ~1.94 equivalents of ruthenium per POM.[123] That is, the authors have not ruled out the possibility that ruthenium is acting as an outer sphere/noncoordinated countercation in the isolated "$Na_{14}[Ru(III)_2Zn_2(H_2O)_2(ZnW_9O_{34})_2]$" complex. Also not known is if adventitious ruthenium could be contributing to the catalytic activity. Quite possibly relevant here is literature showing that Ru(III) incorporation into a $[WZn_3(H_2O)_2(ZnW_9O_{34})_2]^{12-}$ precursor—as the Howell et al.[123] paper uses—can be problematic. For example, such syntheses are known to lead, in the case of what was claimed to be "$[WZnRu^{III}_2(H_2O)(OH)(ZnW_9O_{34})_2]^{11-}$", to what is actually a physical mixture of the $Ru(II)(DMSO)_4Cl_2$ and $WZn_3(H_2O)_2(ZnW_9O_{34})^{12-}$ starting materials.[152] Therefore, additional characterization and stability

dx.doi.org/10.1021/cs4011716 | ACS Catal. 2014, 4, 909–933

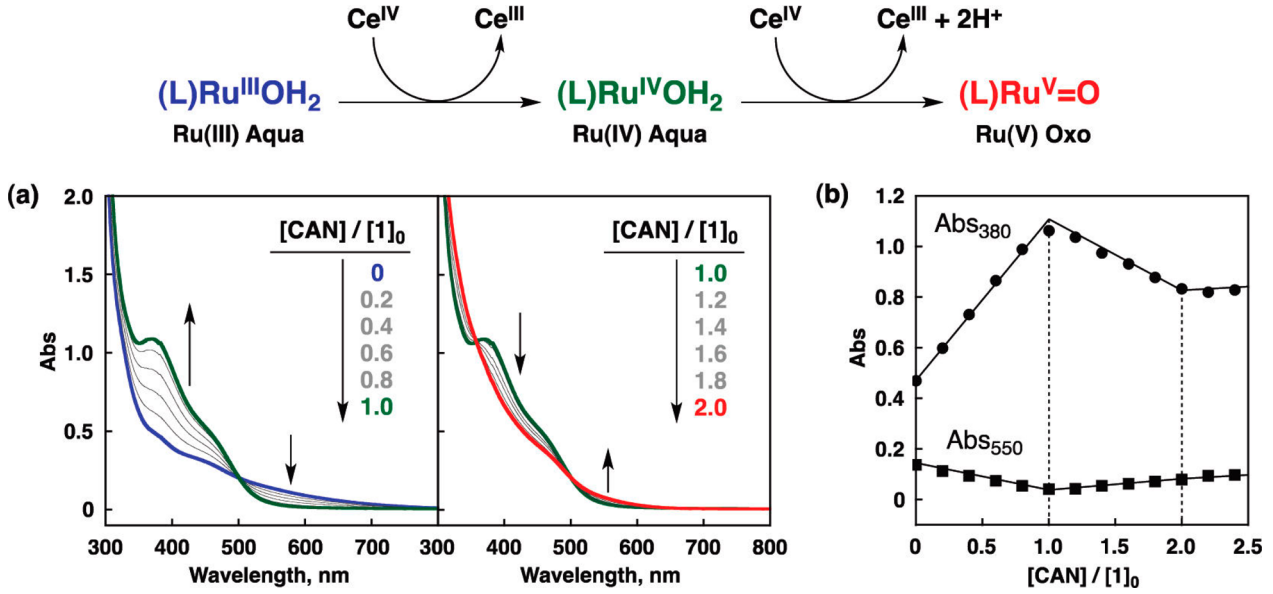

Figure 11. (a) UV−vis spectroscopy of 0.3 mM $[Ru(H_2O)SiW_{11}O_{39}]^{5-}$ upon addition of 0 to 2.5 equivalents of Ce(IV) (i.e., CAN) oxidant. (b) Absorbance changes at 380 and 550 nm plotted as a function of added Ce(IV) equivalents. Coupled with the complementary methods of EPR, resonance Raman, and electrochemical techniques, this example data provides good evidence for a homogeneous POM WOC. Reproduced with permission from ref 76.

studies are needed to provide stronger evidence for both the purity and precise nature of the starting complex, as well as for the true catalyst.

In addition to the multi-Ru POMs described above, single-site ruthenium POMs have also been studied as water oxidation precatalysts. One of the most thorough investigations of a monoruthenium POM starting materials was completed by Murakami et al., where 0.3 mM $[Ru(H_2O)SiW_{11}O_{39}]^{5-}$ or $[Ru(H_2O)GeW_{11}O_{39}]^{5-}$ (Figure 5, vide supra for their structure) was combined with 6.0 mM Ce(IV) oxidant to produce O_2 in up to 90% yields.[76] Characterization of Ru(III), Ru(IV), and Ru(V)-POM intermediates included pH-dependent electrochemical studies, EPR, resonance Raman, and UV−vis spectroscopy (Figure 11). Significantly, addition of two or more Ce(IV) equivalents to the starting POM resulted in the formation of a proposed $[Ru(O)GeW_{11}O_{39}]^{5-}$ species. Kinetic analyses were also conducted and indicate that O_2 evolution kinetics: (i) are first order in the Ru(V)═O species (i.e., the proposed catalyst resting state under oxidizing conditions), (ii) saturate in [Ce(IV)], and (iii) are nearly zero order in $[H^+]$ (although a slight inverse dependence is observed). Multiple controls also support the conclusion of a homogeneous POM WOC, including a lack of O_2 evolution activity when $RuCl_3$, $Ru(acac)_3$ or $[SiW_{11}O_{39}]^{8-}$ were tested as precatalysts. Perhaps the only remaining experiment still needed is to quantify the stability of $[Ru(H_2O)SiW_{11}O_{39}]^{5-}$ and $[Ru(H_2O)GeW_{11}O_{39}]^{5-}$ during and after the catalytic run.

Sadakane and co-workers also investigated $[Ru(H_2O)SiW_{11}O_{39}]^{5-}$ and $[Ru(H_2O)GeW_{11}O_{39}]^{5-}$ as well as $[Ru(H_2O)PW_{11}O_{39}]^{4-}$ ([POM] = 0.3 mM) with 30 mM Ce(IV) oxidation in 0.1 M HNO_3;[84,124] approximately quantitative conversion of Ce(IV) into O_2 was observed over 2 h. These authors did not observe significant O_2 production in control experiments with a variety of precursors, including $[Ru(benzene)Cl_2]_2$, $[PW_{11}O_{39}\{Ru(II)(benzene)(H_2O)\}]^{5-}$, or $[K_7PW_{11}O_{39}]$ plus $[Ru(benzene)Cl_2]_2$. Controls with $RuCl_2(DMSO)_4$, $[K_7PW_{11}O_{39}]$, or $RuCl_2(DMSO)_4$ plus $[K_7PW_{11}O_{39}]$ had O_2 evolution induction periods of a half-hour and produced approximately 3 times less O_2 than did $[Ru(H_2O)PW_{11}O_{39}]^{4-}$. Although the studies of Sadakane did not report any other experiments directly relevant to identifying the true catalyst in their ruthenium POM solutions, it seems plausible that the catalyst is homogeneous since these authors used similar HNO_3 electrolyte and Ce(IV) oxidant conditions comparable to the more extensive studies of Murakami et al.[76]

In summary of this section, Ru-POM water oxidation precatalysts have been studied relatively thoroughly compared to other transition-metal-based POM precursors. Two traits have contributed to this improved understanding. First, ruthenium POMs appear to be more stable than first row transition metal analogues. This increased stability has allowed the ruthenium POMs to be examined using Ce(IV) oxidation in acidic (pH 1 or less) solution; Ce(IV) supplied generally as $[Ce(NO_3)_6](NH_4)_2$ also appears to cause fewer problems with precipitation compared to a $Ru(bpy)_3^{3+}$ oxidant as one might expect from their respective anionic vs cationic charges. This makes in situ and even in operando characterization of ruthenium POMs feasible. The second characteristic which makes ruthenium POMs easier to study is the rich redox chemistry of the active site. Because multiple, reversible electron/proton transfers occur prior to the onset of catalytic activity, these reaction intermediates can be studied and characterized in detail. Despite these advantages, there is clearly a shift in the recent literature toward studying catalysts which incorporate earth-abundant elements—one important trait which ruthenium does not possess.

3.3. Manganese. *3.3.1. Non-POM Manganese Precatalysts.* Homogeneous complexes containing manganese have been studied extensively due to their potential relationship with the biological water oxidation catalyst of photosystem II, which contains a Mn_4 active site. An $L_6Mn_4O_4$ complex (L = diphenylphosphate anion) is one of the few complexes which has been reported to be both a structural and catalytic

dx.doi.org/10.1021/cs4011716 | ACS Catal. 2014, 4, 909−933

mimic of the photosystem II active site.[153,154] Subsequently, Hocking et al. used a combination of EXAFS/XANES, multiple Mn^{2+} starting material controls, and HRTEM to provide strong evidence that a heterogeneous manganese(III/IV) oxide catalyst is formed within the Nafion membrane upon oxidation of the $L_6Mn_4O_4$ starting material.[155] Interestingly, reduction of the heterogeneous MnO_x results in the disappearance of the nanoparticles that are formed concomitantly with what appears to be homogeneous $[Mn(OH_2)_6]^{2+}$. In other words, manganese WOCs appear to be able to cycle between heterogeneous catalysts and homogeneous resting states.

Decomposition of homogeneous manganese coordination complexes, including $(bpy)_2Mn(\mu\text{-}O)_2Mn(bpy)_2$ and $Mn(phen)_3^{2+}$, has also been described when using Ce(IV) oxidation. When the manganese complexes were combined with Ce(IV) in aqueous solution, a mixture of soluble Mn(III), soluble MnO_4^-, and heterogeneous MnO_x were formed although no O_2 was detected.[156] The colloidal MnO_x was characterized by XPS, IR, DLS, TEM, and UV−vis. However, when $(bpy)_2Mn(\mu\text{-}O)_2Mn(bpy)_2$ was supported on clay followed by Ce(IV) addition, O_2 evolution was observed; postreaction IR, XPS, SEM, and XRD characterization indicated the formation of heterogeneous MnO_2 and MnO materials concomitant with loss of the organic bpy ligands. These studies indicate the potentially high instability of manganese complexes to oxidizing conditions, especially in the presence of support materials such as clays.

3.3.2. Manganese POM Precatalysts. All three of the manganese polyoxometalate studies which report water oxidation catalysis are electrochemically driven. It should also be noted that none of these studies quantify O_2 production since this was not the primary focus of these reports; therefore, the reaction being studied is not known definitively for these Mn-POMs. Despite this shortcoming, the techniques used in these studies are relevant to distinguishing between homogeneous and heterogeneous electrocatalysts and are therefore included in the present review.

In 2007, Keita et al. reported the synthesis and electrochemical activity of a $[(Mn(III)(H_2O))_3(SbW_9O_{33})_2]^{9-}$ complex.[87] Cyclic voltammetry studies at a glassy carbon electrode show a reversible Mn(III/IV) redox process followed by an irreversible wave at 1.35 V versus SCE, which is attributed to catalytic water oxidation by a Mn(V) complex. Scan-rate-dependent voltammetry suggests that some of the Mn(III/IV) oxidation is due to adsorbed $[(Mn(III)(H_2O))_3(SbW_9O_{33})_2]^{9-}$. Multiple scans of the POM up to 1.5 V results in a continually increasing catalytic wave, whereas the Mn(III/IV) waves increase only slightly and stabilize after three scans. Due to the complexity of the electrochemical response, the authors used electrochemical quartz crystal microbalance (EQCM) experiments to gain insights into the possibility of MnO_x formation under oxidizing conditions. Consistent with their cyclic voltammetry results, the POM in the Mn(IV) oxidation state adsorbs to the electrode, and reduction to the Mn(II) state results in desorption in the majority, but not all, of the electrode-bound film. The authors suggest this residual film may correspond to MnO_x and is likely responsible for the water oxidation activity. Additional surface characterization was not conducted, however. Even though the identity of the true WOC remains unknown in the case of $[(Mn(III)(H_2O))_3(SbW_9O_{33})_2]^{9-}$, the use of EQCM should prove to be a very useful technique for detecting heterogeneous electrocatalysts.

Two other electrocatalytic water oxidation studies have been reported when starting with manganese POMs. Cyclic voltammetry of $[Mn(III)_3(H_2O)_5(A\text{-}\alpha\text{-}PW_9O_{er})_2]^{9-}$,[88] which is structurally similar to $[(Mn(III)(H_2O))_3(SbW_9O_{33})_2]^{9-}$, shows an apparently catalytic oxidation wave at ~1.1 V versus SCE, proposed by the authors to be water oxidation, but was not investigated further. A catalytic oxidation wave is also observed in $[Mn_{19}(OH)_{12}(SiW_{10}O_{37})_6]^{34-}$ solutions and exhibits a current−overpotential slope of 135 mV/decade with as little as 330 mV of overpotential.[89] Oxidation of $[Mn_{19}(OH)_{12}(SiW_{10}O_{37})_6]^{34-}$ also results in the formation of a thin film on the electrode.

In summary of this section, an important feature of these Mn POMs is that they operate at moderate to low overpotentials and they incorporate earth-abundant catalytic centers. Hence, further characterization of both the POM stability, as well as any in situ formed films, is of interest for all of these manganese POMs.

3.4. Molybdenum. There are no other proposed homogeneous (or to our knowledge heterogeneous) molybdenum WOCs. This is not surprising since molybdenum oxide or polyoxomolybdates typically contain the metal in its highest oxidation state (VI) and the (VI/V) reduction potentials are well below the reversible water oxidation potential. In other words, there is no obvious mechanism for oxidizing water when starting with a molybdenum(VI)-oxo species.

Given the lack of (non-POM-based) Mo WOCs, the cases and claims of molybdenum POMs acting as water oxidation catalysts is something of a curiosity. Hence, there is an additional burden of strong evidence upon researchers claiming Mn POM, or for that matter any Mo-based WOC, be it potentially homogeneous or heterogeneous catalysis.

3.4.1. Molybdenum POM Precatalysts. One study which claims Mo-POM WOCs begins with insoluble POM-$Ru(phen)_3^{2+}$ salts, including $[Ru(II)(phen)_3(CH_3OH)(Mo_6O_{19})]$, $[Ru(II)(phen)_3(C_2H_8N_2)(C_3H_7NO)(Mo_5S_2O_{23})]$, and $[(Ru(II)(phen)_3)_2(CH_3CN)_2(Mo_8O_{26})]$.[157] In the presence of light and 10 mM $S_2O_8^{2-}$, 10 μM POM/photosensitizer suspensions produce O_2 for up to 12 h without significant changes in activity. Powder X-ray diffraction (PXRD) of the materials before and after photocatalysis provide evidence that no significant changes to the bulk of the material occur, although this method would not detect amorphous surface catalysts. To test their hypothesis of a $HO^\bullet$ radical-based reaction mechanism, the authors added hydroquinone, which is a radical scavenger. In the presence of hydroquinone, $[Ru(II)(phen)_3(CH_3OH)(Mo_6O_{19})]$ produces no O_2 under an otherwise standard photochemical reaction. Although the lack of O_2 in this experiment is consistent with a radical mechanism, it is also possible that hydroquinone is simply easier to oxidize than water and therefore reacts preferentially. Additionally, if a radical mechanism involving $HO^\bullet$ is invoked, the authors should also rule out the possibility that the sulfate radical anion ($SO_4^{\bullet-}$)—a byproduct of this particular photochemical system—is not involved directly in the reaction. This problem could be addressed by using ^{18}O-labeled water to verify the source of oxygen in the product O_2. Due to the unprecedented nature of molybdenum WOCs, the most likely WOC in this system involves the $Ru(phen)_3^{3+}$ or its oxidation products. Lay et al. and Creutz and Sutin have proposed water oxidation mechanisms when starting solely with ruthenium polypyridyl complexes to account for O_2 evolved in the absence of other WOCs.[158,159] Determining the catalyst in this case should therefore rely on understanding the stability and speciation of both the POM and photosensitizer materials under the reaction conditions.

dx.doi.org/10.1021/cs4011716 | ACS Catal. 2014, 4, 909−933

Another study of water oxidation catalysis beginning with molybdenum POMs, which arguably could also be classified as cobalt POMs, uses $[Co(III)Mo_6O_{24}H_6]^{3-}$ and $[Co(III)_2Mo_{10}O_{38}H_4]^{6-}$.[106] These POMs are considered molybdenum POMs for the purposes of this review, because the cobalt atoms are internal, core cobalts and contain no terminal aquo, hydroxo, or oxo ligands. Hence, if these intact POMs are indeed homogeneous WOCs, then the oxygen atoms in the O_2 product should not have been coordinated to the cobalt. Photochemical water oxidation with 1−20 μM $[CoMo_6O_{24}H_6]^{3-}$ and $[Co_2Mo_{10}O_{38}H_4]^{6-}$ was investigated in the presence of 0.06 mM $Ru(bpy)_3^{2+}$, 3.0 mM $S_2O_8^{2-}$, and illumination from a 300 W xenon lamp; yields of up to 25% and 20% conversion of persulfate into O_2 are observed. As with other POMs, evidence for POM:$Ru(bpy)_3^{2+}$ precipitation includes saturation kinetics in the O_2 evolution rate beginning at ∼10 μM $[CoMo_6O_{24}H_6]^{3-}$ and 5 μM $[Co_2Mo_{10}O_{38}H_4]^{6-}$. DLS also showed the presence of particles when 40 μM $[Co_2Mo_{10}O_{38}H_4]^{6-}$ was combined with 60 μM $Ru(bpy)_3^{2+}$ but not at lower concentrations. Other DLS experiments did not detect particles in standard postreaction solutions of $[CoMo_6O_{24}H_6]^{3-}$ or $[Co_2Mo_{10}O_{38}H_4]^{6-}$, which had been illuminated for 30 s (i.e., ∼1/20th the length of the normal photochemical reactions employed). A control using 10 μM $Co(NO_3)_2$ under otherwise standard photochemical conditions resulted in the formation of 10−100 nm particles, which were characterized by DLS after 30 s of illumination. No other characterization of these nanoparticles was reported, although literature precedent suggests they are likely CoO_x materials.[134,135] In another control experiment, 20 μM $Co(NO_3)_2$ evolved 7−8 times less O_2 than $[CoMo_6O_{24}H_6]^{3-}$ or $[Co_2Mo_{10}O_{38}H_4]^{6-}$ during a standard 30 min photolysis. It would be interesting to test other, lower concentrations of $Co(NO_3)_2$ in this system since others have observed an O_2 evolution activity *which can depend inversely on the precursor Co^{2+} concentration.*[122] Determining the correct $Co(NO_3)_2$ control in this and other systems ultimately relies on knowing the stability/speciation of the $[CoMo_6O_{24}H_6]^{3-}$ or $[Co_2Mo_{10}O_{38}H_4]^{6-}$ materials in operando, something missing from the above, intriguing system.

3.5. Iridium. *3.5.1. Non-POM Iridium Precatalysts.* The current iridium WOC literature is divided as to whether homogeneous iridium complexes are active WOCs or whether they decompose into heterogeneous IrO_x. Initially, a number of IrCp and IrCp* complexes were reported as homogeneous WOCs.[160−163] Then, in 2010, Grotjahn and co-workers published a pivotal study which found that many of these iridium complexes are initially not active WOCs;[164] instead, greater than 5 equivalents of Ce(IV) are needed to form an active WOC. In operando UV−vis of the Ir complexes plus Ce(IV) is also consistent with the evolution of catalytically active IrO_x materials during the reaction. Lastly, ex situ STEM/EDX revealed the presence of Ir-rich nanoparticles contained in a ceria matrix. Although the true catalyst continues to be debated in iridium plus Ce(IV) systems,[165,166] the study of Grotjahn et al. provides excellent precedent for the in situ formation of active IrO_x nanoparticles in at least certain cases.

Electrochemical studies by Crabtree and co-workers have also investigated distinguishing homogeneous and heterogeneous iridium water oxidation catalysis.[167,168] Investigation of $[Cp^*Ir(H_2O)_3]^{2+}$ and $[Cp^*Ir(2\text{-}(2'\text{-pyridyl})\text{-}2\text{-proponolate})Cl]$ using an electrochemical quartz crystal nanobalance (EQCN) showed that at oxidizing potentials (up to 1.5 V vs NHE) the $[Cp^*Ir(H_2O)_3]^{2+}$ complex electrodeposited a catalytically active, amorphous IrO_x film onto the electrode which contains ∼9% carbon (by EDX); no measurable iridium oxide was deposited onto the electrode for the other iridium complex.[167,168] Therefore, the authors concluded that this EQCN technique can distinguish homogeneous and heterogeneous iridium catalysts, a conclusion with which we concur.

3.5.2. $[(IrCl_4)KP_2W_{20}O_{72}]^{7-}$ Precatalyst. The only example of an iridium polyoxometalate precursor in water oxidation catalysis was reported by Cao et al. in 2009.[77] When 0.02 mM $[(IrCl_4)KP_2W_{20}O_{72}]^{7-}$ is combined with 1.4 mM $Ru(bpy)_3^{3+}$ oxidant at pH 7.2, O_2 yields of up to 30% were observed. In comparison, a control with an equivalent amount of $IrCl_3$ yielded 38% O_2 under otherwise identical conditions. Instability of the starting POM was also observed in the pH 7.2 electrolyte by UV−vis spectroscopy, the iridium dissociating completely from $[(IrCl_4)KP_2W_{20}O_{72}]^{7-}$ within 24 h. Stability of the complex under the reaction conditions was not reported, however. The authors conclude that although the starting POM could be a catalyst, they cannot disprove the possibility of in situ formation of heterogeneous IrO_2 nanoparticle catalysis. Indeed, the combination of $[(IrCl_4)KP_2W_{20}O_{72}]^{7-}$ instability and kinetic competence of the $IrCl_3$ control is most consistent with an in situ formed IrO_x WOC.

3.6. Nickel. *3.6.1. Non-POM Nickel Precatalysts.* Oxidative conversion of aqueous nickel(II) salts and nickel coordination complexes into heterogeneous NiO_x WOCs has been reported by Spiccia and co-workers.[169,170] These studies use a variety of starting materials including $Ni(en)_3^{2+}$, $Ni(NH_3)_6^{2+}$, $Ni(tacn)_2^{2+}$, $Ni(tacn)(OH_2)_3^{2+}$, and $Ni(cyclen)(OH_2)_2^{2+}$, which were oxidized at FTO electrodes to form the nickel oxide films when the potential is scanned up to 1.3 V versus Ag/AgCl in pH 9.2 sodium borate buffer. EXAFS/XANES, SEM, Raman, and EDX characterization of the films indicate the NiO_x materials were similar to other NiOOH catalytic materials. Interestingly, if the electrode potential is scanned only up to 0.85 V versus NHE (i.e., past the first oxidation wave, but prior to catalytic water oxidation) no measurable NiO_x is formed for any of the complexes (except for controls with $Ni(OH_2)_6^{2+}$). This result indicates that stability of a complex prior to catalysis does not guarantee its stability under more oxidizing conditions—a point which is frequently overlooked in the POM WOC literature. Another relevant finding in these studies is the observation of increasing electrocatalytic activity with increasing electroactive surface area of the NiO_x films. Although surface-area-dependent activity is well-known in heterogeneous catalysis, this result reinforces the need to consider and account for the effect of solid catalyst's surface area and numbers of active sites in control experiments aimed at ruling out, or supporting, the presence of heterogeneous WOCs.

3.6.2. $[Ni_5(OH)_6(OH_2)_3(Si_2W_{18}O_{66})]^{12-}$ Precatalyst. A 2010 report by Zhu et al. describes the synthesis of the penta-nickel POM, $[Ni_5(OH)_6(OH_2)_3(Si_2W_{18}O_{66})]^{12-}$, and tests it as a WOC starting material.[78] As was observed for several other POMs, DLS shows the formation of 700−1300 nm particulate precipitate when $[Ni_5(OH)_6(OH_2)_3(Si_2W_{18}O_{66})]^{12-}$ and $Ru(bpy)_3^{2+}$ are combined. If this POM:$Ru(bpy)_3^{2+}$ is filtered from the solution, the filtrate produces no O_2 when testing under standard photochemical conditions (455 nm light, 1.0 mM $Ru(bpy)_3^{2+}$, and 5.0 mM $S_2O_8^{2-}$). Controls using $Ni(NO_3)_2$ showed that filtration followed by standard photochemical testing did result in O_2 evolution—evidence against Ni^{2+} leaching from the Ni-POM prior to catalysis. The precatalytic stability of $[Ni_5(OH)_6(OH_2)_3(Si_2W_{18}O_{66})]^{12-}$ was also followed by UV−vis spectroscopy, DLS, and IR (after crystallization from pH 8 solution) and showed no apparent changes

dx.doi.org/10.1021/cs4011716 | ACS Catal. 2014, 4, 909−933

upon aging in pH 8 borate buffer in experiments which lasted up to 12 h or 2 years.

Evidence consistent with the $\{[Ni_5(OH)_6(OH_2)_3(Si_2W_{18}O_{66})]^{12-}\}$:$[Ru(bpy)_3^{2+}]$ precipitate stability under the photochemical reaction conditions includes three FTIR experiments:[78] (1) characteristic POM IR peaks are present both before and after photocatalysis; (2) nickel hydroxide controls show IR bands at 525 and 3640 cm^{-1} both as an isolated material and when mixed with the Ni−POM in a 9:1 molar ratio; (3) the post reaction IR shows no evidence of the nickel hydroxide bands. Although these experiments are good initial tests, it is not clear whether the nickel hydroxide ($Ni(OH)_2$) control (which was prepared by precipitation of aqueous nickel(II) using KOH) would show the same IR stretches of oxidatively prepared Ni(III)OOH. The authors also assumed that if a NiOOH-containing nanoparticle was formed, that it would be isolated by the centrifugation isolation method and therefore observable in the FTIR spectrum. An alternative explanation is that the catalyst remains in the supernatant.

The authors final argument for a homogeneous nickel POM WOC is that the kinetic traces for photochemical O_2 evolution and dark $Ru(bpy)_3^{3+}$ reduction (i.e., where the reaction is driven by addition of the ruthenium(III) oxidant in the dark) are similar, and the O_2 yields have the same trend for light-driven and dark reactions.[78] Unfortunately, there are at least two possible gaps in this argument. First, O_2 evolution and oxidant loss kinetics can only be rigorously compared when the O_2 yield is near 100% since one cannot know what portion of the oxidant loss corresponds to O_2 evolution and what portion corresponds to side-oxidation reactions. Second, an observation of increasing O_2 yields with increasing [Ni−POM] for both light and dark reactions only requires that the amount of catalyst increases for both these systems when more starting material is used; that is, increasing O_2 evolution rates do not indicate the true catalyst unless they can be correlated with a precise compound/species under the reaction conditions.

4. SUMMARY

Analysis of the WOC literature which uses POM precatalysts reveals several important insights: (i) The majority of studies examine the stability of the starting POM prior to catalysis and then infer the stability of the catalyst under the reaction conditions. In operando quantitative stability, with *error limits*, and speciation studies are badly needed and, therefore, broadly recommended. (ii) With two exceptions,[79,81] the studies which do address whether the POM is present at the end of the reaction do not quantify the stability; instead these studies rely on FTIR, ^{31}P NMR, and PXRD to show the qualitative stability of the POM. Thus, the hypothesized superior stability of POMs under water oxidation conditions has yet to be supported by concrete evidence since the two quantitative studies available at present[79,81] actually report POM instability. (iii) Although in situ tests for particles such as DLS and SAXS are useful, one should also be aware of and report the detection limit of the particles one is attempting to detect when these techniques are used to provide evidence against nanoparticles in the solution. (iv) Development of faster in operando methods of real-time O_2 detection promises to have an important impact on WOC studies. (v) Control experiments are critical to distinguishing homogeneous and heterogeneous WOCs and are greatly underutilized at present. In order to compare a heterogeneous control to a homogeneous precursor, one should also know the approximate number of active sites/surface area of the heterogeneous control catalyst as well as the dependence on that surface area in the observed kinetics. (vi) Understanding the water oxidation kinetics of all possible forms of the (pre)catalyst is crucial to determining which catalyst is active is a particular system. (vii) Reaction conditions can play an important role in determining the identity of the dominant WOC especially when working with only quasi-stable POMs.

Electrochemical studies have several advantages over chemical/photochemical oxidation methods including: (1) Many of the solubility issues associated with $Ru(bpy)_3^{3+}$ oxidation can be avoided since the concentration and identity of the electrolyte can be chosen to maximize POM solubility. (2) Fewer side oxidation reactions are observed in electrochemical systems relative to the common ligand oxidation reactions associated with the $Ru(bpy)_3^{3+}$ oxidant. (3) If heterogeneous materials are deposited onto the electrode during the reaction, then they can be easily isolated from the starting POM solution and can be characterized by a variety of methods including SEM/EDX, XPS, IR. And, (4) the electrochemical potential/driving force for the reaction can be easily varied in order to determine kinetic parameters and to compare different catalysts/controls.

Chemical oxidation methods, on the other hand, have the advantage of interacting with the entire solution instead of only the portion that reaches the electrode/solution interface. That said, there is a pressing need for an uncharged or anionic oxidant that yields a stable, readily quantitated product. In comparison to the broader WOC literature, knowledge of the true catalyst when beginning with POMs is lagging and can be quite challenging in part due to the solubility/stability problems associated with the use of chemical oxidation methods. Again, either new, noncationic oxidants are needed, or electrochemical oxidation methods should be utilized.

An important point is that conceptually solving the "is it homogeneous or heterogeneous catalysis?" question is as simple or as complex as (i) having complete speciation of the precatalyst under the reaction conditions, and then (ii) knowing the kinetic contribution of each species formed. Practically, however, this is much harder than it sounds, especially when micromolar to nanomolar amount of leached metal can form competent catalysts.[66,67,81] Finally, "catalysis is...purely a kinetic phenomenon".[116] This, in turn, means that rigorous, unequivocal identification of the true catalyst for any catalytic reaction is impossible without the requisite kinetic studies. An important corollary here is that a comparison of TOFs, without knowledge of the underlying rate laws, will tend to be a comparison of mechanisms, conditions, and terms in the often different rate laws.[171,172]

Due to the challenges associated with determining the homogeneity or heterogeneity of water oxidation catalysts, development of methods aimed at answering this fundamentally important problem of "who is the true catalyst?" will continue to be highly relevant. Understanding the fundamental properties that control catalyst formation, activity, stability, and lifetime will be important in developing future water oxidation catalysts capable of the stringent requirements needed for sustainable energy storage.

The expectation is that an improved understanding of the actual catalysts in a given water oxidation reaction will help focus and therefore expedite WOC research. Hence, this review of WOCs starting with POMs and how, in our experience, to best and most quickly identify the true catalyst is offered as hopefully one valuable step in the needed focus towards the most active, most long-lived, and overall best water-oxidation catalysts achievable. Finally, to further aid the efforts of anyone striving to identify the true catalyst in their own water oxidation or other catalytic reactions, Table A which follows is provided as a quick-reference guide to the systems that have been discussed in the present review.

dx.doi.org/10.1021/cs4011716 | ACS Catal. 2014, 4, 909−933

APPENDIX

Table A. Summary of Experiments Relevant to Distinguishing Homogeneous and Heterogeneous WOCs When Using POM Precatalysts

POM	oxidant, electrolyte[a]	experiments relevant to distinguishing homogeneous versus heterogeneous catalysis	ref
$[Co_4(H_2O)_2(PW_9O_{34})_2]^{10-}$	$Ru(III)(bpy)_3^{3+}$ in pH 8.0, NaPi and NaBi	No UV−vis or ^{31}P NMR changes observed over 1 month at pH 8. Aging Co_4POM for 3 days did not decrease the O_2 yield whereas controls with aged $Co(NO_3)_2$ decreased to 33.6% O_2 yield. In postreaction solution (where $Ru(bpy)_3^{2+}$ had been precipitated by addition of sodium tetraphenylborate), the ^{31}P NMR spectrum showed the presence of the Co_4POM. CV of Co_4POM plus $Ru(bpy)_3^{2+}$ both before and after reaction with $Ru(bpy)_3^{3+}$ shows an oxidative wave which changes only slightly; controls with $Co(NO_3)_2$ showed a decrease in the postreaction CV (which likely contained CoO_x plus the $Ru(bpy)_3^{2+}$) compared to the prereaction CV.	65
		When Co_4POM is precipitated from the postreaction solution by addition of $Ru(bpy)_3^{2+}$, the IR is consistent with the Co_4POM being present in the precipitate.	
		Addition of 2,2′-bipyridine to the 3.2 μM Co_4POM decreased the O_2 yield from 67 to 48% and decreased the O_2 yield for 13 μM $Co(NO_3)_2$ controls from 80 to 0%. No O_2 was observed for Co_4POM at pH 6.2 but $Co(NO_3)_2$ showed a yield of 35%. Redissolution of the $Ru(bpy)_3^{2+}$-Co_4POM precipitate and addition of $Ru(bpy)_3^{3+}$ showed an O_2 yield of 49%.	
$[Co_4(H_2O)_2(PW_9O_{34})_2]^{10-}$	$h\nu$, $Ru(II)(bpy)_3^{2+}$, $Na_2S_2O_8$ in pH 8, NaBi	No particles observed by dynamic lights scattering or Tyndall effects, under conditions of 1 mM $Ru(bpy)_3^{2+}$, 160 mM NaBi, pH 8, 5 μM Co_4POM, 5 mM $Na_2S_2O_8$.	105
		Sequential photochemical runs, where additional $Na_2S_2O_8$ was added between runs, showed a ∼20% decrease in O_2 yield.	
$[Co_4(H_2O)_2(PW_9O_{34})_2]^{10-}$	$h\nu$, $Ru(II)(bpy)_3^{2+}$, $Na_2S_2O_8$ in pH 8, NaPi	$Co(NO_3)_2$ flash photolysis controls reportedly do not show any observed particles by light scattering. CV of Co_4POM solutions show an anodic peak at ∼1.2 V versus Ag/AgCl which increases with aging time and an irreversible wave is observed above ∼1.3 V.	85
		Flash photolysis showed increasing activity of $Ru(bpy)_3^{3+}$ quenching by Co_4POM solutions with aging of the Co_4POM solutions—the maximum activity corresponds to ∼20% of the initial [Co_4POM] which is reached in about 90 min of aging. Controls with $Co(NO_3)_2$ were reported to consume the photogenerated $Ru(bpy)_3^{3+}$ on a longer time scale.	
$[Co_4(H_2O)_2(PW_9O_{34})_2]^{10-}$	electrochem. 1.14 V versus Ag/AgCl, glassy carbon in pH 8, NaPi	Linear sweep voltammetry shows increasing anodic wave at ∼1.05 V with aging over 3 h. This increasing current occurs concomitantly with a 4.3 ± 0.6% decrease in the 580 nm absorbance of Co_4POM and a 58 ± 2 μM increase in the apparent aqueous [Co^{2+}] which was measured by two methods. Bulk electrolysis of the Co_4POM solution at 1.14 V versus Ag/AgCl (without aging) results in the deposition of a catalytically active film.	66
		The electrodeposited film was removed from the Co_4POM solution and placed into a POM-free solution and maintains all its water oxidation activity. Also, this film contains Co, P, Na, and O as determined by EDX (i.e., no W as would be expected if the film contained the Co_4POM).	
		Bulk electrolysis of the Co_4POM solution at 1.14 V versus Ag/AgCl (without aging) results in an increasing catalytic current with time. Catalytic controls with a 500 μM Co_4POM solution (aged for 3 h) and a 58 μM $Co(NO_3)_2$ solution showed quantitatively identical water oxidation activity (101 ± 12%) during a 5 min bulk electrolysis at 1.14 V versus Ag/AgCl.	
$[Co_4(H_2O)_2(PW_9O_{34})_2]^{10-}$	electrochem. 1.4 V versus Ag/AgCl, glassy carbon in pH 5.8−8.0 NaPi	Co_4POM cyclic voltammograms show onset of an oxidation wave above ∼1.25 V versus Ag/AgCl, whereas controls with CoO_x show a catalytic wave onset of ∼1.05 V. The Co_4POM wave saturates at concentration of ∼5 μM Co_4POM. The $[Co^{2+}]_{apparent}$ in 2.5 μM Co_4POM solutions increases to 0.25 μM during a 1 h aging experiment at pH 8. The [Co^{2+}] also increases by 50 ± 34 μM during the electrolysis. Repeated bulk electrolysis (for 60s at 1.4 V vs Ag/AgCl, repeated three times on the same solution) resulted in a [Co^{2+}] = 825 nM.	81
		Comparison of the pre- and postreaction Co_4POM solutions revealed that during a 60 s bulk electrolysis, the [Co_4POM] decreases by 2.7 ± 7.3% and 9.4 ± 5.1% at pH 8.0 and 5.8.	
		The Co_4POM solutions and CoO_x-coated electrodes show a pH-oxidation wave dependence of −36 and −66 mV/pH unit (i.e., for each pH unit increase, the oxidation wave moves by 36 and 66 mV to a more negative potential, respectively). Bulk electrolysis controls at 1.4 V versus Ag/AgCl using the predetermined amount of Co^{2+} (i.e., 0.2 μM) do not account for the observed water oxidation activity in Co_4POM solutions. Controls with deposited CoO_x reveal that 0.45−0.58 nmols and 1.0−1.5 nmols of CoO_x, at pH 8.0 and 5.8, could account for observed activity in Co_4POM solutions.	
$[Co_4(H_2O)_2(PW_9O_{34})_2]^{10-}$	$Ru(III)(bpy)_3^{3+}$ and $h\nu$, $Ru(II)(bpy)_3^{2+}$, $Na_2S_2O_8$ in NaPi and NaBi pH 6.2−9	The dissociated [Co^{2+}] = 0.07 μM starting with 2 μM Co_4POM in pH 8 sodium borate, as determined by stripping voltammetry and ICP-MS. UV−vis showed Co_4POM has lower stability in phosphate buffer compared to borate buffer. DLS of postphotocatalytic Co_4POM reactions showed no observable particles, whereas controls using $Co(NO_3)_2$ precursors did show particles.	67

dx.doi.org/10.1021/cs4011716 | ACS Catal. 2014, 4, 909−933

Table A. continued

POM	oxidant, electrolyte[a]	experiments relevant to distinguishing homogeneous versus heterogeneous catalysis	ref
		Extraction of the postphotocatalytic POM solution with toluene/THpANO_3 resulted in complete loss of activity. Control extractions showed that extraction before POM addition and photocatalysis did not affect O_2 evolution. Control with Co^{2+} did not extract the Co^{2+} or affect subsequent photocatalysis.	
		Kinetics using either 2 μM Co_4POM or 0.1 μM $Co(NO_3)_2$ plus 2 μM Co_4POM showed the same $Ru(bpy)_3^{3+}$ loss rate within 5%. A control with 0.5 μM showed the same or slower $Ru(bpy)_3^{3+}$ loss rate compared to 2 μM Co_4POM. A photocatalytic control with 0.15 μM $Co(NO_3)_2$ produced the same amount of O_2 as a control with no catalyst. A photocatalytic control with 2 μM $Co(NO_3)_2$ gave an O_2 yield =40.8 $\pm$ 0.5% compared to 2 μM Co_4POM which gave a 24.2 $\pm$ 0.1% yield. Multiple other $Co(NO_3)_2$ andCoO_x controls were conducted.	
$[Co_4(H_2O)_2(PW_9O_{34})_2]^{10-}$	$Ru(III)(bpy)_3^{3+}$ in pH 7.2, NaPi	A $[Ru(bpy)_3^{2+}]_3[Co_4(H_2O)_2(PW_9O_{34})_2^{10-}]_2$ precipitate is formed with a $K_{sp} = (8 \pm 7) \times 10^{-25}$ M^5.	117
		$Co(NO_3)_2$ controls show a first order dependence on precursor concentration, whereas Co_4POM shows $[Co_4POM]^{1\rightarrow 0}$ kinetics with respect to the initial POM concentration; this behavior is consistent with Co_4POM being removed from solution via a $[Ru(bpy)_3^{2+}]_3[Co_4(H_2O)_2(PW_9O_{34})_2^{10-}]_2$ precipitate. The initial rate of 2,2′-bipyridine ligand oxidation followed the same trends as the initial water oxidation rate for Co_4POM solutions, but was independent of the initial $[Co(NO_3)_2]$ in control experiments. That is, Co_4POM solutions appear to catalyze ligand oxidation, whereas $Co(NO_3)_2$ solution do not.	
		Controls with $Co(NO_3)_2$ showed decreasing yields with increasing $Ru(bpy)_3^{3+}$: Co^{2+} (54−18%), whereas the Co_4POM shows increasing O_2 yields with increasing $Ru(bpy)_3^{3+}/Co_4$POM ratios which peaks at a ratio of 500:1 and 22% yield.	
$[Co^{III}Co^{II}(H_2O)W_{11}O_{39}]^{7-}$	hν, $Ru(II)(bpy)_3^{2+}$, $Na_2S_2O_8$, and $Ru(III)(bpy)_3^{3+}$ in pH 8.0−10.0, NaBi, NaPi, NaCi	$[Co^{II}Co^{II}(H_2O)W_{11}O_{39}]^{8-}$ (i.e., the one electron reduction product of the starting POM) decomposes rapidly at the pH of the reactions. No observed particles in $[Co^{III}Co^{II}(H_2O)W_{11}O_{39}]^{7-}$ solutions by DLS after 10 min of reaction (conditions not given), whereas reactions containing 0.1 to 1 mol % $Co(NO_3)_2$ ($[Co(NO_3)_2] + [Co_2POM] = 15$ μM) produced observable particles both before and after photochemical reactions. The authors noted differences in the CVs between the POM and $Co(NO_3)_2$, although the catalytic wave onset is very similar. UV−vis band is stable over 10 min at pH 9.0 although no error bars were given.	68
		Reaction solutions of $[Co^{II}Co^{II}(H_2O)W_{11}O_{39}]^{8-}$ are also active in the water oxidation reaction. Control with 45 nM $Co(NO_3)_2$ showed no observable photo-oxidation activity. Hole scavenging kinetics did not vary with aging the POM solution (1−60 min aging time).	
		Only ∼40% of initial activity is observed when the POM is isolated and retested. Isolation is achieved by precipitating with acetone followed by centrifugation.	
$\{Co_9(H_2O)_6(OH)_3(HPO_4)_2$- $(PW_9O_{34})_3\}^{16-}$	electrochem., 1.41 V versus NHE,FTO and NaClO in pH 7 and 8, NaPi	During electrolysis, the POM concentration decreases by ∼15% and 30% in the absence and presence of bipyridine, as judged by UV−vis spectroscopy. In the presence of bipyridine, a pink precipitate forms during bulk electrolysis of the POM. For NaClO oxidation experiments, no change in the UV−vis spectrum was observed, and dynamic light scattering showed the same result before and after the experiment	79
		Bulk electrolysis of 1 mM POM for 1 h resulted in formation of a catalytic film which contained cobalt and phosphate, as determined by SEM/EDX. The pink precipitate formed during bulk electrolysis of the POM in the presence of bpy was reported to be a $[Co(bpy)_3^{3+}][POM]$ salt and was characterized by IR. In NaClO oxidation experiments, the POM can be recovered from the solution by crystallization or precipitation (as judged by IR and XRD).	
		At 15 °C, the NaClO plus POM reaction appears slightly sigmoidal. Repeated additions of NaClO to the POM shows the TOF and yield after each addition (for five additions) is the same within experimental error. If 2,2′-bipyridine was added to the POM solution before electrolysis, the oxidation current decreases by ∼50-fold, and no film was visible by SEM/EDX and no residual activity was observed on the electrode. The electrochemical onset of oxidation occurs at 0.75 and 1.10 V in the absence and presence of bipyridine. Addition of 10 equivalents of bipyridine to the POM plus NaClO oxidation does not significantly change the O_2 yields or kinetics with additions of NaClO occurring at 0, 84, 108, and 131 h.	
$Cs_{15}K[Co_9(H_2O)_6(OH)_3-$ $(HPO_4)_2(PW_9O_{34})_3]$-carbon paste	electrochem. 1.5 V versus NHE carbon paste in pH 7.0, NaPi	IR spectroscopy and XRD shows the same peaks for Co_9−POM before and after 8 h 1.5 V electrolysis.	102
		Controls were conducted with Co_3O_4 at a variety of loading. Furthermore, 20× the molar amount of cobalt in the form of Co_3O_4 has about half the current of the Co_9−POM. At pH 1, Co_3O_4 shows the same current as carbon paste background; $Co(NO_3)_2$ controls show decreasing activity with increasing amounts of 17.5−52.5 μmols.	
$[\{Ru_3O_3(H_2O)Cl_2\}$-$(SiW_9O_{34})]^{7-}$ and $[Co_4(H_2O)_2(SiW_9O_{34})_2]^{12-}$	hν, $Ru(II)(bpy)_3^{2+}$, $Na_2S_2O_8$ in xpH 5.8, Na_2SiF_6 buffer	A 3.5% and 25% decrease in the UV−vis absorbance bands of $[\{Ru_3O_3(H_2O)Cl_2\}(SiW_9O_{34})]^{7-}$ and $[Co_4(H_2O)_2(SiW_9O_{34})_2]^{12-}$ were observed over 150−180 min at pH 5.8. $[\{Ru_3O_3(H_2O)Cl_2\}(SiW_9O_{34})]^{7-}$ is stable under illumination (but not catalytic conditions) for 3 h.The Ru_3POM-$Ru(bpy)_3^{2+}$ and Co_4POM complexes precipitate, can be isolated from the solution by centrifugation and maintain the characteristic IR bands of the Ru_3POM and Co_4POM.O_2 evolution kinetics appear slightly sigmoidal. Control experiments with $RuCl_3$ gave no observed O_2. Controls with Co^{2+} salts were conducted. After centrifugation of the $Ru(bpy)_3^{2+}$-Ru_3POM solution, the supernatant contains no residual water oxidation activity. Both the precipitated $Ru(bpy)_3^{2+}$−	69
		Ru_3POM and $Ru(bpy)_3^{2+}$- Co_4POM can be resuspended in solution while maintaining water oxidation activity.	

dx.doi.org/10.1021/cs4011716 | ACS Catal. 2014, 4, 909−933

Table A. continued

POM	oxidant, electrolyte[a]	experiments relevant to distinguishing homogeneous versus heterogeneous catalysis	ref
$[Co_4(\mu\text{-}OH)(H_2O)_{3-}(Si_2W_{19}O_{70})]^{11-}$	hν, Ru(II)(bpy)$_3^{2+}$, $Na_2S_2O_8$ in pH 7.2–9.0, NaPi and NaBi	Estimated 5.5 equiv of aqueous Co^{2+} dissociates over 40 days (UV–vis). POM decomposes to $[Co(H_2O)SiW_{11}O_{39}]^{6-}$. Sigmoidal O_2 evolution kinetics at pH 7.2. TON decreases with aging (3–4 weeks)	70, 71
$Na_9H_5[Co_2Bi_2(\alpha\text{-B-}CoW_9O_{34})_2]$ and $Na_9H_5[Co_2Bi_2(\beta\text{-B-}CoW_9O_{34})_2]$	electrochem., glassy carbon and hν, Ru(II)(bpy)$_3^{2+}$, $Na_2S_2O_8$ in pH 7.4, NaPi	A 0.25 mM solution of either POM does not show an electrochemical oxidation wave during 3 h of aging at pH 7.4.	86
$[Ti_{12}O_{15}(O^iPr)_{17}]^+$-$[(CoBr)_6Ti_{15}O_{24}(O^iPr)_{18}(Br)]^-$ and $[(CoI)Ti_{11}O_{14}(O^iPr)_{17}]$	electrochem. 1.35 V versus NHE, FTO in pH 7.0, Pi buffer	SEM/EDX shows the presence of porous islands of the precursor before bulk electrolysis composed of 5.8% cobalt and 0% phosphorus. After catalysis, the islands contain 1.1% and 9.0% cobalt and phosphorus, and the interstitial space between the island contains 8.24% and 4.81%—consistent with in situ formed CoO_x.	110
$[Hpy]_2\{[Co(4,4'\text{-}Hbpy)_2(H_2O)_2][SiCoW_{11}O_{39}]\}$	electrochem. carbon paste in pH 4.5, NaOAc	N/A	149
$[Ru_4(\mu\text{-}O)_4(\mu\text{-}OH)_2(H_2O)_4(\gamma\text{-}SiW_{10}O_{36})_2]^{10-}$	Ce(IV) in pH 0.6	UV–vis shows reversible protonation of POM over pH range of 0.6–2.0 (pK_a = 3.62). This protonation/deprotonation is concentration independent, and the FTIR spectrum is unchanged during this titration. The 443 nm absorption band changes only slightly over 4 days at pH 0.6. Ce(IV) (8 equiv) was added to the POM, allowed to sit for 1 h, the POM was precipitated by Cs^+ addition, and collected by filtration; the IR and resonance Raman spectra appear qualitatively the same as the unreacted sample. (Note: most catalytic reactions were run with ~500–1000 equiv Ce(IV)) O_2 evolution is first-order in [POM]. Control with $K_4Ru_2OCl_{10}$ showed 20 min induction period, ~10× slower O_2 evolution, and 8× lower O_2 yield.	72
$[Ru_4(\mu\text{-}O)_4(\mu\text{-}OH)_2(H_2O)_4(\gamma\text{-}SiW_{10}O_{36})_2]^{10-}$	Ce(IV) and electrochem. (glassy carbon or Pt) 1.15 V versus SSCE	Characterized POM WOC intermediates by CV, UV–vis, EPR, and resonance Raman; data are consistent with oxidation states for the tetra-ruthenium core ranging from $Ru(IV)_4$ to $Ru(V)_4$. Ru_4–POM has nearly identical XANES Ru K-edge and Ru–O bond distance (1.98 Å) compared to RuO_2.	64, 104
$[Ru_4(\mu\text{-}O)_4(\mu\text{-}OH)_2(H_2O)_4(\gamma\text{-}SiW_{10}O_{36})_2]^{10-}$	Ru(bpy)$_3^{3+}$ in pH 7.2, NaPi	UV–vis shows two reversible protonation equilibria between pH 2.5–7.5. The electrochemical response of the POM was reported at pH 1.0 and showed several reversible ruthenium redox waves. At pH 7, an electro-catalytic wave is observed above 900 mV versus Ag/AgCl; when the POM and Ru(bpy)$_3^{2+}$ are combined, the Ru(III/II)(bpy)$_3^{3+/2+}$ couple becomes less chemically reversible as the [POM] increases. Controls with $Ru(III)Cl_3$ in the presence and absence of $[\gamma\text{-}SiW_{10}O_{36}]^{8-}$ showed Ru(bpy)$_3^{3+}$ reduction rates which were 100 times slower than in the presence of the POM.	73
$[Ru_4(\mu\text{-}O)_4(\mu\text{-}OH)_2(H_2O)_4(\gamma\text{-}SiW_{10}O_{36})_2]^{10-}$	Ru(bpy)$_3^{3+}$ in pH 7.2, NaPi	Reversible oxidation/reduction between core oxidation states of $(Ru(IV)_2Ru(V)_2)$ and $(Ru(IV)_2Ru(III)_2)$ using both electrochemical and chemical (Ce(IV) and Sn(II)) oxidants/reductants. UV–vis and CV does not change over several months at room temperature and pH 3–4; slow decomposition is seen in 0.1 M HCl solution. No particles are seen in postreaction solution by SAXS and DLS. Proposed rate law for oxidant consumption: $-d(Ru(bpy)_3^{3+})/dt = 4k_{cat}[POM]1/(1 + [Ru(bpy)_3^{2+}]/(K[Ru(bpy)_3^{3+}]))$. Reaction depends on Ru(bpy)$_3^{3+}$/ Ru(bpy)$_3^{2+}$ ratio, but not on intitial [Ru(bpy)$_3^{3+}$]. Control with $RuCl_3$ gave O_2 yield of <11% which is about 5 times less than for the POM. Addition of bpy does not change the O_2 yield within experimental error. Addition of potassium decreases O_2 yield by 50%.	74
$[Ru_4(\mu\text{-}O)_4(\mu\text{-}OH)_2(H_2O)_4(\gamma\text{-}SiW_{10}O_{36})_2]^{10-}$	electrochem., glassy carbon in 0.1 M HCl or 0.05 M H_2SO_4	Measured ten electrochemical redox potentials for the POM by AC voltammetry. Ru(IV,IV,V,V)/Ru(IV,V,V,V) and Ru(IV,V,V,V)/Ru(V,V,V,V) potentials were measured to be 1.15 and 1.32 V versus Ag/AgCl in 0.05 M H_2SO_4. Electron-transfer rates were reported for most of the redox processes. Potassium cations increase the electron transfer rates.	82
$[Ru_4(\mu\text{-}O)_4(\mu\text{-}OH)_2(H_2O)_4(\gamma\text{-}SiW_{10}O_{36})_2]^{10-}$	hν, Ru(II)(bpy)$_3^{2+}$, $Na_2S_2O_8$ or hν, TiO_2/Ru(4,4′-diphosphonate-2,2′-bipyridine)(bpy)$_2^{2+}$ in pH 7, Pi	Flash photolysis experiments yield a bimolecular rate constant of $(2.1 \pm 0.4) \times 10^9$ $M^{-1}s^{-1}$ for the Ru(bpy)$_3^{3+}$ + POM reaction. Caveat: no O_2.	120
$[Ru_4(\mu\text{-}O)_4(\mu\text{-}OH)_2(H_2O)_4(\text{-}SiW_{10}O_{36})_2]^{10-}$	hν, $[Ru(II)\{(\mu\text{-dpp})Ru(II)(bpy)_2\}_3]^{8+}$, $Na_2S_2O_8$ in pH 7.2, KPi	Reaction is zero order in photosensitizer and persulfate for up to 80% of reaction. System also active in pH 5.8 $Na_2SiF_6/Na_2B_4O_7$ buffer. Ru(bpy)$_3^{2+}$ precipitate formed. Increasing [POM] from 2.5 to 5.0 μM resulted in no increase in O_2 production. O_2 evolution rate scales approximately with initial [Ru(bpy)$_3^{2+}$] and $[Na_2S_2O_8]$. A control with $RuCl_3$ yielded no measurable O_2. A RuO_2 control yielded O_2 evolution rates which were 10–20× lower than the POM.	118
$[Ru_4(\mu\text{-}O)_4(\mu\text{-}OH)_2(H_2O)_4(\gamma\text{-}SiW_{10}O_{36})_2]^{10-}$	hν, Ru(II)(bpy)$_3^{2+}$, $Na_2S_2O_8$ in pH 7.2, NaPi	At concentrations above 5 μM POM, a POM-electrode could be cycled at least 9 times between 1 and 1.6 V versus Ag/AgCl without significant changes in response.	119
MWCNT/PAMAM/$[Ru_4\text{-}(H_2O)_4(\mu\text{-}O)_4(\mu\text{-}OH)_2(\gamma\text{-}SiW_{10}O_{36})_2]^{10-}$, where MWCNT/PAMAM are polyamidoamine functionalized multiwalled carbon nanotubes	electrochem. 1.1–1.6 V versus Ag/AgCl on ITO in pH 7, Pi		83

dx.doi.org/10.1021/cs4011716 | ACS Catal. 2014, 4, 909–933

Table A. continued

POM	oxidant, electrolyte[a]	experiments relevant to distinguishing homogeneous versus heterogeneous catalysis	ref
$[(\gamma\text{-}PW_{10}O_{36})_2Ru_4O_5(OH)\text{-}(H_2O)_4]^{9-}$	hν, $Ru(II)(bpy)_3^{2+}$, $Na_2S_2O_8$ in pH 5.8, Na_2SiF_6	Two reversible protonation equilibria occur at ∼pH 3. Seven reversible ruthenium redox waves are observed for core oxidation states of $(Ru(IV)_2Ru(V)_2)$ to $(Ru(II)Ru(III)_3)$ over pH 0 to 7.	75
		O_2 evolution rate does not appear to depend strongly on initial [POM] although the overall O_2 yield does depend on the initial [POM]. O_2 evolution kinetics look slightly sigmoidal at 5.1 μM POM.	
		$[Ru_4(\mu\text{-}O)_4(\mu\text{-}OH)_2(H_2O)_4(\gamma\text{-}SiW_{10}O_{36})_2]^{10-}$ gave an O_2 yield =40% compared to 25% for $[(\gamma\text{-}PW_{10}O_{36})_2Ru_4O_5(OH)(H_2O)_4]^{9-}$.	
$[Ru(III)_2Zn_2(H_2O)_2\text{-}(ZnW_9O_{34})_2]^{14-}$	electrochem. 0.5−1.05 V versus SHE on Au in pH 8, Pi	Controls with di-ZnPOM and $[PW_{11}O_{39}Ru(III)(H_2O)]^{4-}$ showed no O_2 evolution activity. Tafel analysis gives a 120 mV/decade slope (i.e., twice that typical of RuO_2).	123
$[Ru(H_2O)SiW_{11}O_{39}]^{5-}$ and $[Ru(H_2O)GeW_{11}O_{39}]^{5-}$	Ce(IV) in 0.1−0.55 M HNO_3	Pourbaix diagrams characterize the ruthenium POM redox potentials as a function of potential and pH. The Ru(IV) and Ru(V) POM oxidation states were also characterized by UV−vis, EPR, and resonance Raman (note that only UV−vis was in operando).	76
		O_2 was not evolved in controls using $RuCl_3$, $Ru(acac)_3$, or $[SiW_{11}O_{39}]^{8-}$. O_2 yield of up to 90% were reported for the POM. Ce(IV) loss kinetics was reported as a function [Catalyst], pH, and [CAN]; reaction is first-order in POM, approximately zero order in $[H^+]$, and shows saturation kinetics for Ce(IV).	
$[PW_{11}O_{39}Ru(III)(H_2O)]^{4-}$, $[SiW_{11}O_{39}Ru(III)(H_2O)]^{5-}$, $[GeW_{11}O_{39}Ru(III)(H_2O)]^{5-}$	Ce(IV) in pH 1, HNO_3	Pourbaix diagram indicates that the Ru(V/VI) couple occurs near the reversible water oxidation potential.	84
		Controls with $[Ru(benzene)Cl_2]_2$, $[PW_{11}O_{39}\{Ru(II)(benzene)(H_2O)\}^{5-}$, and $[K_7PW_{11}O_{39}]$ + $[Ru(benzene)Cl_2]_2$, did not show significant amounts of O_2 evolution. O_2 evolution kinetics are slightly sigmoidal for $[PW_{11}O_{39}Ru(III)(H_2O)]^{4-}$ and $[SiW_{11}O_{39}Ru(III)(H_2O)]^{5-}$.	
$[PW_{11}O_{39}Ru(III/II)\text{-}(DMSO)]^{4-/5-}$	Ce(IV) in pH 1, HNO_3	Controls with $RuCl_2(DMSO)_4$, $[K_7PW_{11}O_{39}]$, and $RuCl_2(DMSO)_4$ plus $[K_7PW_{11}O_{39}]$, showed induction periods of ∼0.5 h, and O_2 yields, which were ∼3 times less than $[PW_{11}O_{39}Ru(II)(DMSO)]^{5-}$.	124
$[(Mn(III)(H_2O))_3\text{-}(SbW_9O_{33})_2]^{9-}$	electrochem. 1.345 V versus SCE, glassy carbon in pH 6, NaOAc	CV shows oxidation peak at 1.345 V which is attributed to Mn(V) and electrocatalytic water oxidation; the Mn(IV/III) reduction wave remains chemically reversible. CV indicates adsorption of the POM to the electrode. The oxidation peak currents become larger and the peaks shift to more negative potentials upon cycling the electrode from −0.9 to 1.5 V versus SCE. Bulk electrolysis of the $Mn(II)_3$POM at 0.8 V results in 6.3 electrons passed concomitant with solution color becoming brown.	87
		EQCM indicates deposition of a film at the same potential as the Mn(IV/III) oxidation wave. This film can be removed by reversing the potential negative of the Mn(IV/III) redox potential. Repeated cycling indicates that a small portion of the deposited film remains attached to the electrode; the authors suggest this could be a MnO_x film. Mn(V) oxidation wave was also observed in NaPi buffer at pH 6.	
$[Mn(III)_3(H_2O)_5(A\text{-}\alpha\text{-}PW_9O_{er})_2]^{9-}$	electrochem. 1.1−1.3 V versus SCE, glassy carbon in pH 5, NaPi	CV shows two oxidation peaks (0.55 and 0.78 vs SCE). The peaks become shaper and shift to slightly more negative potentials when the electrode is cycled four times between −0.6 and 1.0 V; authors suggest this is due to MnO_x deposition.	88
$[Mn_{19}(OH)_{12}(SiW_{10}O_{37})_6]^{34-}$	electrochem. ∼0.9−1.25 V versus SCE, glassy carbon in pH 5, NaOAc	CV shows two reversible waves at 0.5 and 0.74 V. Bulk electrolysis at 0.83 V results in passage of 2.00 ± 0.005 electrons per Mn. The electrode can be subjected to hundreds of cycles without deactivation. A film deposits on the electrode surface during water oxidation electrolysis and cycling experiments.	89
		Tafel slope of 135 ± 10 mV/decade	
$[Ru(II)(phen)_3(CH_3OH)\text{-}(Mo_6O_{19})]$ $[Ru(II)(phen)_3(C_2H_8N_2)\text{-}(C_3H_7NO)(Mo_5S_2O_{23})]$ $[Ru(II)(phen)_3(CH_3CN)_2\text{-}(Mo_8O_{26})]$	hν, $Na_2S_2O_8$	PXRD does not show significant changes when comparing pre- and postphotocatalysis POM samples.	157
$[CoMo_6O_{24}H_6]^{3-}$ and $[Co_2Mo_{10}O_{38}H_4]^{6-}$	hν, $Ru(II)(bpy)_3^{2+}$, $Na_2S_2O_8$ in pH 8.0, NaBi	POMs showed no particles by DLS after reaction. Control with 10 μM $Co(NO_3)_2$ showed particles by DLS post reaction.	106
		Single control with 20 μM $Co(NO_3)_2$ which showed ∼8× lower activity than POMs.	
$[(IrCl_4)KP_2W_{20}O_{72}]^{7-}$	$Ru(bpy)_3^{3+}$ in pH 7.2, NaPi	Complete dissociation (>99%) of an $[IrCl_4(H_2O)_2^-$ unit from the POM occurs over 24 h at pH 6.5 or 7.2, as determined by UV−vis and ^{31}P NMR. Control with $IrCl_3$ gave slightly higher O_2 yield (38%) compared to the POM (30%).	77
$[Ni_5(OH)_6(OH_2)_3\text{-}(Si_2W_{18}O_{66})]^{12-}$	hν, $Ru(II)(bpy)_3^{2+}$, $Na_2S_2O_8$	DLS shows 700−1300 nm particles prior to the reaction. Prior to addition of $Ru(bpy)_3^{2+}$, the POM UV−vis spectrum is stable for at least 12 h in pH 8 solution and can be recrystallized after two years in solution. A nickel-borate film forms on electrode surfaces above 1.1 V.	78
		FTIR of the pre- and postreaction POM-$Ru(bpy)_3^{2+}$ material appeared nearly identical (note, the reaction was run at 25× larger scale). An FTIR peak observed at 3640 cm^{-1} for a $Ni(OH_2)_2$ material was not observed in the postreaction POM solution.	
		Reported O_2 evolution kinetics for light driven experiments and $Ru(bpy)_3^{3+}$ reduction kinetics for dark experiments. Filtration of the precatalysis solution followed by irradiation yields no O_2. A control with 1 μM $Ni(NO_3)_2$ + $Ru(bpy)_3^{2+}$ with filtration, did yield O_2 upon illumination.	

[a]NaPi, NaBi, NaCi, and NaOAc are sodium phosphate, sodium borate, sodium carbonate, and sodium acetate buffers.

dx.doi.org/10.1021/cs4011716 | ACS Catal. 2014, 4, 909−933

AUTHOR INFORMATION

Corresponding Author

*E-mail: rfinke@lamar.colostate.edu.

Funding

This work was supported in part by the Chemical Sciences, Geosciences, and Biosciences Division, Office of Basic Energy Sciences, Office of Science, U.S. Department of Energy, Grant DE-FG02−03ER15453 and the National Science Foundation grant CHE-0611588.

Notes

The authors declare no competing financial interest.

ACKNOWLEDGMENTS

J.J.S. thanks the Department of Energy (DOE) Office of Science for a graduate fellowship. The authors thank Prof. Craig Hill and co-workers for supplying a preprint of reference 67.

ABBREVIATIONS

WOC, water oxidation catalyst; POM, polyoxometalate; Co_4POM, $[Co_4(H_2O)_2(PW_9O_{34})_2]^{10-}$; Co_9POM, $\{Co_9(H_2O)_6(OH)_3(HPO_4)_2(PW_9O_{34})_3\}^{16-}$

REFERENCES

(1) Thayer, A. M. *Chem. Eng. News* **2013**, *91*, 64−68.
(2) Crabtree, R. H. *Chem. Rev.* **2012**, *112*, 1536−1554.
(3) Widegren, J. A.; Finke, R. G. *J. Mol Catal. A: Chem.* **2003**, *198*, 317−341.
(4) Phan, N. T. S.; Van Der Sluys, M.; Jones, C. W. *Adv. Synth. Catal.* **2006**, *348*, 609−679.
(5) Alley, W. M.; Hamdemir, I. K.; Johnson, K. A.; Finke, R. G. *J. Mol. Catal. A: Chem.* **2010**, *315*, 1−27.
(6) Artero, V.; Fontecave, M. *Chem. Soc. Rev.* **2013**, *42*, 2338−2356.
(7) Fukuzumi, S.; Hong, D. *Eur. J. Inorg. Chem.* **2013**, DOI: 10.1002/ejic.201300684.
(8) Lewis, N. S.; Nocera, D. G. *Proc. Natl. Acad. Sci. U.S.A.* **2006**, *103*, 15729−15735.
(9) Cook, T. R.; Dogutan, D. K.; Reece, S. Y.; Surendranath, Y.; Teets, T. S.; Nocera, D. G. *Chem. Rev.* **2010**, *110*, 6474−6502.
(10) Ruttinger, W.; Dismukes, G. C. *Chem. Rev.* **1997**, *97*, 1−24.
(11) Betley, T. A.; Wu, Q.; Van Voorhis, T.; Nocera, D. G. *Inorg. Chem.* **2008**, *47*, 1849−1861.
(12) Liu, F.; Concepcion, J. J.; Jurss, J. W.; Cardolaccia, T.; Templeton, J. L.; Meyer, T. J. *Inorg. Chem.* **2008**, *47*, 1727−1752.
(13) Dau, H.; Limberg, C.; Reier, T.; Risch, M.; Roggan, S.; Strasser, P. *ChemCatChem* **2010**, *2*, 724−761.
(14) Cady, C. W.; Crabtree, R. H.; Brudvig, G. W. *Coord. Chem. Rev.* **2008**, *252*, 444−455.
(15) Sala, X.; Romero, I.; Rodriguez, M.; Escriche, L.; Llobet, A. *Angew. Chem., Int.Ed.* **2009**, *48*, 2842−2852.
(16) Yagi, M.; Kaneko, M. *Chem. Rev.* **2001**, *101*, 21−35.
(17) Liu, X.; Wang, F. *Coord. Chem. Rev.* **2012**, *256*, 1115−1136.
(18) Wasylenko, D. J.; Palmer, R. D.; Berlinguette, C. P. *Chem. Commun.* **2013**, *49*, 218−227.
(19) Du, P.; Eisenberg, R. *Energy Environ. Sci.* **2012**, *5*, 6012−6021.
(20) McDaniel, N. D.; Bernhard, S. *Dalton Trans.* **2010**, *39*, 10021−10030.
(21) Song, C. *Catal. Today* **2006**, *115*, 2−32.
(22) Morris, A. J.; Meyer, G. J.; Fujita, E. *Acc. Chem. Res.* **2009**, *42*, 1983−1994.
(23) Dubois, M. R.; Dubois, D. L. *Acc. Chem. Res.* **2009**, *42*, 1974−1982.
(24) Benson, E. E.; Kubiak, C. P.; Sathrum, A. J.; Smieja, J. M. *Chem. Soc. Rev.* **2009**, *38*, 89−99.
(25) Olah, G. A.; Goeppert, A.; Surya Prakash, G. K. *J. Org. Chem.* **2009**, *74*, 487−498.
(26) Herrero, C.; Quaranta, A.; Leibl, W.; Rutherford, A. W.; Aukauloo, A. *Energy Environ. Sci.* **2011**, *4*, 2353−2365.
(27) Tinker, L. L.; McDaniel, N. D.; Bernhard, S. *J. Mater. Chem.* **2009**, *19*, 3328−3337.
(28) Tran, P. D.; Artero, V.; Fontecave, M. *Energy Environ. Sci.* **2010**, *3*, 727−747.
(29) Brimblecombe, R.; Dismukes, G. C.; Swiegers, G. F.; Spiccia, L. *Dalton Trans.* **2009**, 9374−9384.
(30) Yagi, M.; Syouji, A.; Yamada, S.; Komi, M.; Yamazaki, H.; Tajima, S. *Photochem. Photobiol. Sci.* **2009**, *8*, 139−147.
(31) Andreiadis, E. S.; Chavarot-Kerlidou, M.; Fontecave, M.; Artero, V. *Photochem. Photobiol.* **2011**, *87*, 946−964.
(32) Young, K. J.; Martini, L. A.; Milot, R. L.; Snoeberger, R. C., III; Batista, V. S.; Schmuttenmaer, C. A.; Crabtree, R. H.; Brudvig, G. W. *Coord. Chem. Rev.* **2012**, *256*, 2503−2520.
(33) Swierk, J. R.; Mallouk, T. E. *Chem. Soc. Rev.* **2013**, *42*, 2357−2387.
(34) Walter, M. G.; Warren, E. L.; McKone, J. R.; Boettcher, S. W.; Mi, Q.; Santori, E. A.; Lewis, N. S. *Chem. Rev.* **2010**, *110*, 6446−6473.
(35) Balzani, V.; Moggi, L.; Manfrin, M. F.; Bolletta, F.; Gleria, M. *Science* **1975**, *189*, 852−856.
(36) Bard, A. J.; Fox, M. A. *Acc. Chem. Res.* **1995**, *28*, 141−145.
(37) Gust, D.; Moore, T. A.; Moore, A. L. *Faraday Discuss.* **2012**, *155*, 9−26.
(38) Geletii, Y. V.; Yin, Q.; Hou, Y.; Huang, Z.; Ma, H.; Song, J.; Besson, C.; Luo, Z.; Cao, R.; O'Halloran, K. P.; Zhu, G.; Zhao, C.; Vickers, J. W.; Ding, Y.; Mohebbi, S.; Kuznetsov, A. E.; Musaev, D. G.; Lian, T.; Hill, C. L. *Isr. J. Chem.* **2011**, *51*, 238−246.
(39) Han, Z. G.; Bond, A. M.; Zhao, C. *Sci. China* **2011**, *54*, 1877−1887.
(40) Lv, H.; Geletii, Y. V.; Zhao, C.; Vickers, J. W.; Zhu, G.; Luo, Z.; Song, J.; Lian, T.; Musaev, D. G.; Hill, C. L. *Chem. Soc. Rev.* **2012**, *41*, 7572−7589.
(41) Sartorel, A.; Bonchio, M.; Campagna, S.; Scandola, F. *Chem. Soc. Rev.* **2013**, *42*, 2262−2280.
(42) Pope, M. T. *Heteropoly and Isopoly Oxometalates*; Springer: Berlin, 1983.
(43) Nlate, S.; Jahier, C. *Eur. J. Inorg. Chem.* **2013**, 1606−1619.
(44) Dolbecq, A.; Mialane, P.; Keita, B.; Nadjo, L. *J. Mater. Chem.* **2012**, *22*, 24509−24521.
(45) Mizuno, N.; Kamata, K.; Yamaguchi, K. *Top. Organomet. Chem.* **2011**, *37*, 127−160.
(46) Mizuno, N.; Yamaguchi, K.; Kamata, K. *Catal. Surv. Asia* **2011**, *15*, 68−79.
(47) Berardi, S.; Carraro, M.; Sartorel, A.; Modugno, G.; Bonchio, M. *Isr. J. Chem.* **2011**, *51*, 259−274.
(48) Brégeault, J.-M.; Vennat, M.; Salles, L.; Piquemal, J.-Y.; Mahha, Y.; Briot, E.; Bakala, P. C.; Atlamsani, A.; Thouvenot, R. *J. Mol. Catal. A: Chem.* **2006**, *250*, 177−189.
(49) Keita, B.; Nadjo, L. *J. Mol. Catal. A: Chem.* **2007**, *262*, 190−215.
(50) Zheng, S.-T.; Yang, G.-Y. *Chem. Soc. Rev.* **2012**, *41*, 7623−7646.
(51) Oms, O.; Dolbecq, A.; Mialane, P. *Chem. Soc. Rev.* **2012**, *41*, 7497−7536.
(52) Izarova, N. V.; Pope, M. T.; Kortz, U. *Angew. Chem., Int. Ed.* **2012**, *51*, 9492−9510.
(53) Putaj, P.; Lefebvre, F. *Coord. Chem. Rev.* **2011**, *255*, 1642−1685.
(54) Hutin, M.; Long, D.-L.; Cronin, L. *Isr. J. Chem.* **2011**, *51*, 205−214.
(55) Finke, R. G.; Droege, M. W. *J. Am. Chem. Soc.* **1984**, *106*, 7274−7277.
(56) Finke, R. G.; Rapko, B.; Saxton, R. J.; Domaille, P. J. *J. Am. Chem. Soc.* **1986**, *108*, 2947−2960.
(57) Scwartz, J. *Acc. Chem. Res.* **1985**, *18*, 302−308.
(58) Platt, J. R. *Science* **1964**, *146*, 347−353.
(59) Chamberlain, T. C. *Science* **1965**, *148*, 754−759.
(60) Meunier, F.; Daturi, M. *Catal. Today* **2006**, *113*, 1−2. Meunier, F.; Daturi, M. *Catal. Today* **2006**, *113*, 1−2.
(61) Tinnemans, S. J.; Mesu, J. G.; Kervinen, K.; Visser, T.; Nijhuis, T. A.; Beale, A. M.; Keller, D. E.; van der Eerden, A. M. J.; Weckhuysen, B. M. *Catal. Today* **2006**, *113*, 3−15.

(62) Contant, R.; Ciabrini, J.-P. *J. Chem. Res. Synop.* **1982**, 50−51.
(63) Contant, R. *J. Chem. Res. Synop.* **1984**, 120−121.
(64) Sartorel, A.; Miró, P.; Salvadori, E.; Romain, S.; Carraro, M.; Scorrano, G.; Di Valentin, M.; Llobet, A.; Bo, C.; Bonchio, M. *J. Am. Chem. Soc.* **2009**, *131*, 16051−16053.
(65) Yin, Q.; Tan, J. M.; Besson, C.; Geletii, Y. V.; Musaev, D. G.; Kuznetsov, A. E.; Luo, Z.; Hardcastle, K. I.; Hill, C. L. *Science* **2010**, *328*, 342−345.
(66) Stracke, J. J.; Finke, R. G. *J. Am. Chem. Soc.* **2011**, *133*, 14872−14875.
(67) Vickers, J. W.; Lv, H.; Sumliner, J. M.; Zhu, G.; Luo, Z.; Musaev, D. G.; Geletii, Y. V.; Hill, C. L. *J. Am. Chem. Soc.* **2013**, *135*, 14110−14118.
(68) Song, F.; Ding, Y.; Ma, B.; Wang, C.; Wang, Q.; Du, X.; Fu, S.; Song, J. *Energy Environ. Sci.* **2013**, *6*, 1170−1184.
(69) Car, P.-E.; Guttentag, M.; Baldridge, K. K.; Alberto, R.; Patzke, G. R. *Green Chem.* **2012**, *14*, 1680−1688.
(70) Zhu, G.; Geletii, Y. V.; Kögerler, P.; Schilder, H.; Song, J.; Lesne, S.; Zhao, C.; Hardcastle, K. I.; Musaev, D. G.; Hill, C. L. *Dalton Trans.* **2012**, *41*, 2084−2090.
(71) Zhu, G.; Lv, H.; Vickers, J. W.; Geletii, Y. V.; Luo, Z.; Song, J.; Huang, Z.; Musaev, D. G.; Hill, C. L. *Proc. SPIE* **2011**, *8109*, 81090A.
(72) Sartorel, A.; Carraro, M.; Scorrano, G.; De Zorzi, R.; Geremia, S.; McDaniel, N. D.; Bernhard, S.; Bonchio, M. *J. Am. Chem. Soc.* **2008**, *130*, 5006−5007.
(73) Geletii, Y. V.; Botar, B.; Kögerler, P.; Hillesheim, D. A.; Musaev, D. G.; Hill, C. L. *Angew. Chem., Int. Ed.* **2008**, *47*, 3896−3899.
(74) Geletii, Y. V.; Besson, C.; Hou, Y.; Yin, Q.; Musaev, D. G.; Quiñonero, D.; Cao, R.; Hardcastle, K. I.; Proust, A.; Kögerler, P.; Hill, C. L. *J. Am. Chem. Soc.* **2009**, *131*, 17360−17370.
(75) Besson, C.; Huang, Z.; Geletii, Y. V.; Lense, S.; Hardcastle, K. I.; Musaev, D. G.; Lian, T.; Proust, A.; Hill, C. L. *Chem. Commun.* **2010**, *46*, 2784−2786.
(76) Murakami, M.; Hong, D.; Suenobu, T.; Yamaguchi, S.; Ogura, T.; Fukuzumi, S. *J. Am. Chem. Soc.* **2011**, *133*, 11605−11613.
(77) Cao, R.; Ma, H.; Geletii, Y. V.; Hardcastle, K. I.; Hill, C. L. *Inorg. Chem.* **2009**, *48*, 5596−5598.
(78) Zhu, G.; Glass, E. N.; Zhao, C.; Lv, H.; Vickers, J. W.; Geletii, Y. V.; Musaev, D. G.; Song, J.; Hill, C. L. *Dalton Trans.* **2012**, *41*, 13043−13049.
(79) Goberna-Ferrón, S.; Vigara, L.; Soriano-López, J.; Galán-Mascarós, J. R. *Inorg. Chem.* **2012**, *51*, 11707−11715.
(80) Kirk, A. D.; Riske, W.; Lyon, D. K.; Rapko, B.; Finke, R. G. *Inorg. Chem.* **1989**, *28*, 792−797.
(81) Stracke, J. J.; Finke, R. G. *ACS Catal.* **2013**, *3*, 1209−1219.
(82) Lee, C.-Y.; Guo, S.-X.; Murphy, A. F.; McCormac, T.; Zhang, J.; Bond, A. M.; Zhu, G.; Hill, C. L.; Geletii, Y. V. *Inorg. Chem.* **2012**, *51*, 11521−11532.
(83) Toma, F. M.; Sartorel, A.; Iurlo, M.; Carraro, M.; Parisse, P.; Maccato, C.; Rapino, S.; Gonzalez, B. R.; Amenitsch, H.; Ros, T. D.; Casalis, L.; Goldoni, A.; Marcaccio, M.; Scorrano, G.; Scoles, G.; Paolucci, F.; Prato, M.; Bonchio, M. *Nat. Chem.* **2010**, *2*, 826−831.
(84) Ogo, S.; Miyamoto, M.; Ide, Y.; Sano, T.; Sadakane, M. *Dalton Trans.* **2012**, *41*, 9901−9907.
(85) Natali, M.; Berardi, S.; Sartorel, A.; Bonchio, M.; Campagna, S.; Scandola, F. *Chem. Commun.* **2012**, *48*, 8808−8810.
(86) Guo, D.; Teng, S.; Liu, Z.; You, W.; Zhang, L. *J. Clust. Sci.* **2013**, *24*, 549−558.
(87) Keita, B.; Mialane, P.; Sécheresse, F.; de Oliveira, P.; Nadjo, L. *Electrochem. Commun.* **2007**, *9*, 164−172.
(88) Al-Oweini, R.; Bassil, B. S.; Palden, T.; Keita, B.; Lan, Y.; Powell, A. K.; Kortz, U. *Polyhedron* **2013**, *52*, 461−466.
(89) Bassil, B. S.; Ibrahim, M.; Al-Oweini, R.; Asano, M.; Wang, Z.; van Tol, J.; Dalal, N. S.; Choi, K.-Y.; Biboum, R. N.; Keita, B.; Nadjo, L.; Kortz, U. *Angew. Chem., Int. Ed.* **2011**, *50*, 5961−5964.
(90) Rong, C.; Anson, F. C. *Anal. Chem.* **1994**, *66*, 3124−3130.
(91) Keita, B.; Contant, R.; Abdeljalil, E.; Girard, F.; Nadjo, L. *Electrochem. Commun.* **2000**, *2*, 295−300.
(92) Keita, B.; Abdeljalil, E.; Nadjo, L.; Contant, R.; Belghiche, R. *Langmuir* **2006**, *22*, 10416−10425.
(93) The overpotential, or electrochemical driving force, is defined as the difference between the electrode potential and the reversible potential for the reaction of interest. For the water oxidation reaction, the overpotential can be calculated using the equation: $\eta = E - (1.23 - 0.059 \cdot \mathrm{pH})$ V, where E is the potential of the electrode versus NHE and $(1.23 - 0.059 \cdot \mathrm{pH})$ V is the reversible potential for water oxidation.
(94) Gileadi, E. *Electrode Kinetics for Chemists, Chemical Engineers, and Materials Scientists*; Wiley-VCH: New York, 1993.
(95) Fedetov, M. A.; Maksimovskaya, R. I. *J. Sruct. Chem.* **2006**, *47*, 952−978.
(96) Chen, Y.-G.; Gong, J.; Qu, L.-Y. *Coord. Chem. Rev.* **2004**, *248*, 245−260.
(97) Howarth, O. W. *Mol. Eng.* **1993**, *3*, 131−140.
(98) Contant, R. *Can. J. Chem.* **1987**, *65*, 568−573.
(99) Zhu, Z.; Tain, R.; Rhodes, C. *Can. J. Chem.* **2003**, *81*, 1044−1050.
(100) Jorris, T. L.; Kozik, M.; Casan-Pastor, N.; Domaille, P. J.; Finker, R. G.; Miller, W. K.; Baker, L. C. W. *J. Am. Chem. Soc.* **1987**, *109*, 7402−7408.
(101) Ohlin, C. A.; Harley, S. J.; McAlpin, J. G.; Hocking, R. K.; Mercado, B. Q.; Johnson, R. L.; Villa, E. M.; Fidler, M. K.; Olmstead, M. M.; Spiccia, L.; Britt, R. D.; Casey, W. H. *Chem.—Eur. J.* **2011**, *17*, 4408−4417.
(102) Soriano-López, J.; Goberna-Ferrón, S.; Vigara, L.; Carbó, J. J.; Poblet, J. M.; Galán-Mascarós, J. R. *Inorg. Chem.* **2013**, *52*, 4753−4755.
(103) Wachs, I. E.; Roberts, C. A. *Chem. Soc. Rev.* **2010**, *39*, 5002−5017.
(104) Piccinin, S.; Sartorel, A.; Aquilanti, G.; Goldoni, A.; Bonchio, M.; Fabris, S. *Proc. Natl. Acad. Sci. U.S.A.* **2013**, *110*, 4917−4922.
(105) Huang, Z.; Luo, Z.; Geletii, Y. V.; Vickers, J. W.; Yin, Q.; Wu, D.; Hou, Y.; Ding, Y.; Song, J.; Musaev, D. G.; Hill, C. L.; Lian, T. *J. Am. Chem. Soc.* **2011**, *133*, 2068−2071.
(106) Tanaka, S.; Annaka, M.; Sakai, K. *Chem. Commun.* **2012**, *48*, 1653−1655.
(107) Kaxauba, K.; McKnight, D.; Connah, M. T.; McNeil-Watson, F. K.; Nobbmann, U. *J. Nanopart. Res.* **2008**, *10*, 823−829.
(108) Wyatt, P. J. *Anal. Chim. Acta* **1993**, *272*, 1−40.
(109) Katsoulis, D. E.; Pope, M. T. *J. Am. Chem. Soc.* **1984**, *106*, 2737−2738.
(110) Lai, Y.-H.; Lin, C.-Y.; Lv, Y.; King, T. C.; Steiner, A.; Muresan, N. M.; Gan, L.; Wright, D. S.; Reisner, E. *Chem. Commun.* **2013**, *49*, 4331−4333.
(111) Goldstein, J. I.; Newbury, D. E.; Joy, D. C.; Lyman, C. E.; Echlin, P.; Lifshin, E.; Saywer, L.; Michael, J. R. *Scanning Electron Microscopy and X-Ray Microanalysis*, 3rd ed.; Kluwer: New York, 2003.
(112) Baer, D. R.; Engelhard, M. H. *J. Electron Spectrosc. Relat. Phenom.* **2010**, *178*−*179*, 415−432.
(113) Wang, Y.; Weinstock, I. A. *Chem. Soc. Rev.* **2012**, *41*, 7479−7496.
(114) Hagen, C. M.; Widegren, J. A.; Maitlis, P. M.; Finke, R. G. *J. Am. Chem. Soc.* **2005**, *127*, 4423−4432.
(115) Miras, H. N.; Wilson, E. F.; Cronin, L. *Chem. Commun.* **2009**, *45*, 1297−1311.
(116) Halpern, J. *Inorg. Chim. Acta* **1981**, *50*, 11−19.
(117) Stracke, J. J.; Finke, R. G. *ACS Catal.* **2014**, *4*, 79−89.
(118) Puntoriero, F.; La Ganga, G.; Sartorel, A.; Carraro, M.; Scorrano, G.; Bonchio, M.; Campagna, S. *Chem. Commun.* **2010**, *46*, 4725−4727.
(119) Geletii, Y. V.; Huang, Z.; Hou, Y.; Musaev, D. G.; Lian, T.; Hill, C. L. *J. Am. Chem. Soc.* **2009**, *131*, 7522−7523.
(120) Orlandi, M.; Argazzi, R.; Sartorel, A.; Carraro, M.; Scorrano, G.; Bonchio, M.; Scandola, F. *Chem. Commun.* **2010**, *46*, 3152−3154.
(121) Brunschwig, B. S.; Chou, M. H.; Creutz, C.; Sutin, N. *J. Am. Chem. Soc.* **1983**, *105*, 4832−4833.
(122) Ghosh, P.; Brunschwig, B. S.; Chou, M.; Creutz, C.; Sutin, N. *J. Am. Chem. Soc.* **1984**, *106*, 4772−4783.
(123) Howells, A. R.; Sankarraj, A.; Shannon, C. *J. Am. Chem. Soc.* **2004**, *126*, 12258−12259.

(124) Sadakane, M.; Rinn, N.; Moroi, S.; Kitatomi, H.; Ozeki, T.; Kurasawa, M.; Itakura, M.; Hayakawa, S.; Kato, K.; Miyamoto, M.; Ogo, S.; Ide, Y.; Sano, T. *Z. Anorg. Allg. Chem.* **2011**, *637*, 1467−1474.
(125) Bayram, E.; Linehan, J. C.; Fulton, J. L.; Roberts, J. A. S.; Szymczak, N. K.; Smurthwaite, T. D.; Ozkar, S.; Balasubramanian, M.; Finke, R. G. *J. Am. Chem. Soc.* **2011**, *133*, 18889−18902.
(126) Elizarova, G. L.; Matvienko, L. G.; Lozhkina, N. V.; Parmon, V. N.; Zamarev, K. I. *React. Kinet. Catal. Lett.* **1981**, *16*, 191−194.
(127) Elizarova, G. L.; Matvienko, L. G.; Lozhkina, N. V.; Parmon, V. N. *React. Kinet. Catal. Lett.* **1983**, *22*, 49−53.
(128) Kim, T. V.; Elizarova, G. L.; Parmon, V. N. *React. Kinet. Catal. Lett.* **1984**, *26*, 57−60.
(129) Elizarova, G. L.; Matvienko, L. G.; Lozhkina, N. V.; Parmon, V. N. *React. Kinet. Catal. Lett.* **1984**, *26*, 62−72.
(130) Elizarova, G. L.; Kim, T. V.; Matvienko, L. G.; Parmon, V. N.; Nkitin, V. I. *React. Kinet. Catal. Lett.* **1986**, *31*, 455−459.
(131) Elizarova, G. L.; Matvienko, L. G.; Parmon, V. N. *J. Mol. Catal.* **1987**, *43*, 171−181.
(132) Pestunova, O. P.; Elizarova, G. L.; Parmon, V. N. *Kinet. Catal.* **2000**, *41*, 375−384.
(133) Elizarova, G. L.; Zhidomirov, G. M.; Parmon, V. N. *Catal. Today* **2000**, *58*, 71−88.
(134) Shevchenko, D.; Anderlund, M. F.; Thapper, A.; Styring, S. *Energy Environ. Sci.* **2011**, *4*, 1284−1287.
(135) Risch, M.; Shevchenko, D.; Anderlund, M. F.; Styring, S.; Heidkamp, J.; Lange, K. M.; Thapper, A.; Zaharieva, I. *Int. J. Hydrog. Energy* **2012**, *37*, 8878−8888.
(136) Hong, D.; Jung, J.; Park, J.; Yamada, Y.; Suenobu, T.; Lee, Y.-M.; Nam, W.; Fukuzumi, S. *Energy Environ. Sci.* **2012**, *5*, 7606−7616.
(137) Shafirovich, V. Y.; Strelets, V. V. *New J. Chem.* **1978**, *2*, 199−201.
(138) Kanan, M. W.; Nocera, D. G. *Science* **2008**, *321*, 1072−1075.
(139) Kanan, M. W.; Surendranath, Y.; Nocera, D. G. *Chem. Soc. Rev.* **2009**, *38*, 109−114.
(140) Lutterman, D. A.; Surendranath, Y.; Nocera, D. G. *J. Am. Chem. Soc.* **2009**, *131*, 3838−3839.
(141) Surendranath, Y.; Dinca, M.; Nocera, D. G. *J. Am. Chem. Soc.* **2009**, *131*, 2615−2620.
(142) Kanan, M. W.; Yano, J.; Surendranath, Y.; Dinca, M.; Yachandra, V. K.; Nocera, D. G. *J. Am. Chem. Soc.* **2010**, *132*, 13692−13701.
(143) McAlpin, J. G.; Surendranath, Y.; Dinca, M.; Stich, T. A.; Stoian, S. A.; Casey, W. H.; Nocera, D. G.; Britt, R. D. *J. Am. Chem. Soc.* **2010**, *132*, 6882−6883.
(144) Surendranath, Y.; Kanan, M. W.; Nocera, D. G. *J. Am. Chem. Soc.* **2010**, *132*, 16501−16509.
(145) Risch, M.; Khare, V.; Zaharieva, I.; Gerencser, L.; Chernev, P.; Dau, H. *J. Am. Chem. Soc.* **2009**, *131*, 6936−6937.
(146) Gerken, J. B.; Landis, E. C.; Hamers, R. J.; Stahl, S. S. *ChemSusChem* **2010**, *3*, 1179−1179.
(147) Gerken, J. B.; McAlpin, J. G.; Chen, J. Y. C.; Rigsby, M. L.; Casey, W. H.; Britt, R. D.; Stahl, S. S. *J. Am. Chem. Soc.* **2011**, *133*, 14431−14442.
(148) Kirner, J. T.; Stracke, J. J.; Gregg, B. A.; Finke R. G. *ACS Appl. Mater. Interfaces*, submitted.
(149) Wang, H.; You, W.; Meng, B.; Sun, X.; Cheng, H.; Shan, W. *J. Clust. Sci.* **2010**, *21*, 857−865.
(150) Mills, A.; Russel, T. *J. Chem. Soc. Faraday Trans.* **1991**, *87*, 313−318.
(151) Collin, J. P.; Sauvage, J. P. *Inorg. Chem.* **1986**, *25*, 135−141.
(152) Morris, A. M.; Anderson, O. P.; Finker, R. G. *Inorg. Chem.* **2009**, *48*, 4411−4420.
(153) Brimblecombe, R.; Kolling, D. R. J.; Bond, A. M.; Dismukes, G. C.; Swiegers, G. F.; Spiccia, L. *Inorg. Chem.* **2009**, *48*, 7269−7279.
(154) Brimblecombe, R.; Koo, A.; Dismukes, G. C.; Swiegers, G. F.; Spiccia, L. *J. Am. Chem. Soc.* **2010**, *132*, 2892−2894.
(155) Hocking, R. K.; Brimblecombe, R.; Chang, L.-Y.; Singh, A.; Cheah, M. H.; Glover, C.; Casey, W. H.; Spiccia, L. *Nat. Chem.* **2011**, *3*, 461−466.
(156) Najafpour, M. M.; Moghaddam, A. N. *Dalton Trans.* **2012**, *41*, 10292−10297.
(157) Gao, J.; Cao, S.; Tay, Q.; Liu, Y.; Yu, L.; Ye, K.; Mun, P. C. S.; Li, Y.; Rakesh, G.; Loo, S. C. J.; Chen, Z.; Zhao, Y.; Xue, C.; Zhang, Q. *Sci. Rep.* **2013**, *3*, 1853.
(158) Lay, P. A.; Sasse, W. H. F. *Inorg. Chem.* **1985**, *24*, 4707−4710.
(159) Creutz, C.; Sutin, N. *Proc. Natl. Acad. Sci. U.S.A.* **1975**, *72*, 2858−2862.
(160) McDaniel, N. D.; Coughlin, F. J.; Tinker, L. L.; Bernhard, S. *J. Am. Chem. Soc.* **2008**, *130*, 210−217.
(161) Hull, J. F.; Balcells, D.; Blakemore, J. D.; Incarvito, C. D.; Eisenstein, O.; Brudvig, G. W.; Crabtree, R. H. *J. Am. Chem. Soc.* **2009**, *131*, 8730−8731.
(162) Blakemore, J. D.; Schley, N. D.; Balcells, D.; Hull, J. F.; Olack, G. W.; Incarvito, C. D.; Eisenstein, O.; Brudvig, G. W.; Crabtree, R. H. *J. Am. Chem. Soc.* **2010**, *132*, 16017−16029.
(163) Savini, A.; Bellachioma, G.; Ciancaleoni, G.; Zuccaccia, C.; Zuccaccia, D.; Macchioni, A. *Chem. Commun.* **2010**, *46*, 9218−9219.
(164) Grotjahn, D. B.; Brown, D. B.; Martin, J. K.; Marelius, D. C.; Abadjian, M.-C.; Tran, H. N.; Kalyuzhny, G.; Vecchio, K. S.; Specht, Z. G.; Cortes-Llamas, S. A.; Mirando-Soto, V.; van Niekerk, C.; Moore, C. E.; Rheingold, A. L. *J. Am. Chem. Soc.* **2011**, *133*, 19024−19027.
(165) Savini, A.; Bucci, A.; Bellachioma, G.; Rocchigiani, L.; Zuccaccia, C.; Llobet, A.; Macchioni, A. *Eur. J. Inorg. Chem.* **2013**, DOI: 10.1002/ejic.201300530.
(166) Hintemair, U.; Sheehan, S. W.; Parent, A. R.; Ess, D. H.; Richens, D. T.; Vaccaro, P. H.; Brudvig, G. W.; Crabtree, R. H. *J. Am. Chem. Soc.* **2013**, *135*, 10837−10851.
(167) Schley, N. D.; Blakemore, J. D.; Subbaiyan, N. K.; Incarvito, C. D.; D'Souza, F.; Crabtree, R. H.; Brudvig, G. W. *J. Am. Chem. Soc.* **2011**, *133*, 10473−10481.
(168) Blakemore, J. D.; Schley, N. D.; Olack, G. W.; Incarvito, C. D.; Brudvig, G. W.; Crabtree, R. H. *Chem. Sci.* **2011**, *2*, 94−98.
(169) Singh, A.; Chang, S. L. Y.; Hocking, R. K.; Bach, U.; Spiccia, L. *Catal. Sci. Technol.* **2013**, *3*, 1728−1732.
(170) Singh, A.; Chang, S. L. Y.; Hocking, R. K.; Bach, U.; Spiccia, L. *Energy Environ. Sci.* **2013**, *6*, 579−586.
(171) Kozuch, S.; Martin, J. M. *ACS Catal.* **2012**, *2*, 2787−2794.
(172) Lente, G. *ACS Catal.* **2013**, *3*, 381−382.